



Nordisk kernesikkerhedsforskning  
Norrænar kjarnöryggisrannsóknir  
Pohjoismainen ydinturvallisuustutkimus  
Nordisk kjernesikkerhetsforskning  
Nordisk kärnsäkerhetsforskning  
Nordic nuclear safety research

NKS-154  
ISBN 978-87-7893-217-4

---

# Analysis of Loads and Fluid-Structure Interactions in a Condensation Pool

Antti Timperi, Timo Pättikangas and Jarto Niemi  
VTT, Technical Research Centre of Finland

April 2007

## Abstract

A simplified direct contact condensation model was implemented into the Volume of Fluid model of the Fluent CFD code. Transient three-dimensional test runs for the POOLEX experiments, where steam is blown into a water pool were performed. The model was found to provide too small condensation rate for steam when compared to experiments. In addition, the calculated back and forth oscillation of the steam water interface was much smaller than in the experiments. The model was found to be numerically quite robust. The discrepancies of the simulation, such as the too small condensation rate, could be to some extent cured by making improvements into the condensation model.

As an alternative estimation method of thermohydraulic loads in condensation pools, the SILA code based on potential flow theory, was taken into use. SILA solves the pressure distribution caused by oscillating bubbles in a pool, and is easier to use and more flexible than Method of Images studied earlier. SILA has been modified for pools without an inner cylinder and test simulations for the POOLEX water pool were performed.

The MpCCI FSI coupling software employs an explicit coupling scheme, which results in numerical instability in the case of the POOLEX facility. In order to improve stability, ways for implementing an implicit coupling scheme with MpCCI were examined. It was found that such a scheme is difficult to achieve without access to the source codes. An implicit coupling scheme is expected to be available with MpCCI in forthcoming years.

A method was developed which can be used for analysing two-way FSI problems realistically by using only one-way coupling of CFD and structural analysis codes. In the method, the mass of the fluid is accounted for in the structural motion by adding the fluid to the structural model as an acoustic medium. Validity of the method was examined with promising results mathematically by an order of magnitude analysis and by comparing numerical results with a full two-way calculation in a simple test case and with a POOLEX experiment. The method has certain restrictions, the most important being that structural displacements have to be sufficiently small. These restrictions do not seem to be too limiting for modeling the POOLEX facility or a real pressure suppression pool. The method may have significance in many other applications as well where structural motion is small but the added mass effect of fluid is significant.

## Key words

CFD, FEM, fluid-structure interaction, steam injection, pressure suppression pool

NKS-154

ISBN 978-87-7893-217-4

Electronic report, April 2007

The report can be obtained from

NKS Secretariat

NKS-776

P.O. Box 49

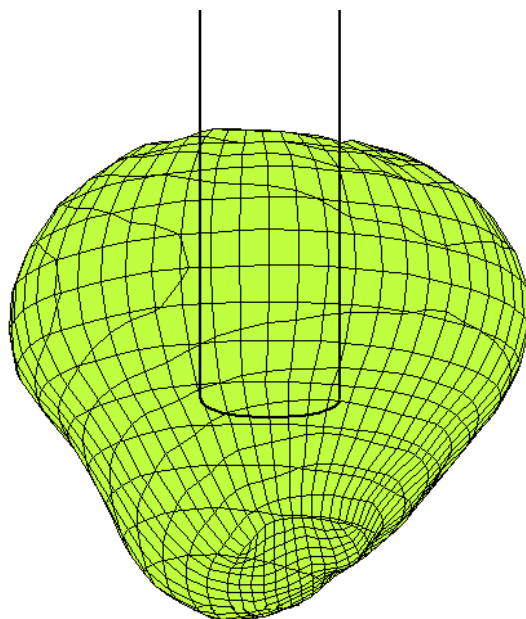
DK - 4000 Roskilde, Denmark

Phone +45 4677 4045

Fax +45 4677 4046

[www.nks.org](http://www.nks.org)

e-mail [nks@nks.org](mailto:nks@nks.org)





## Analysis of Loads and Fluid-Structure Interactions in a Condensation Pool

Authors

Antti Timperi, Timo Pättikangas and Jarto Niemi

Confidentiality

Public

Report's title Analysis of Loads and Fluid-Structure Interactions in a Condensation Pool	
Customer, contact person, address VYR, NKS	Order reference
Project name SAFIR / INTELI / INPUT	Project number/Short name 3573-1.4
Author(s) Antti Timperi, Timo Pättikangas and Jarto Niemi	Pages 41/
Keywords CFD, FEM, fluid-structure interaction, steam injection, pressure suppression pool	Report identification code VTT-R-01365-07
<p><b>Summary</b></p> <p>A simplified direct contact condensation model was implemented into the Volume Of Fluid model of the Fluent CFD code. Transient three-dimensional test runs for the POOLEX experiments, where steam is blown into a water pool were performed. The model was found to provide too small condensation rate for steam when compared to experiments. In addition, the calculated back and forth oscillation of the steam water interface was much smaller than in the experiments. The model was found to be numerically quite robust. The discrepancies of the simulation, such as the too small condensation rate, could be to some extent cured by making improvements into the condensation model.</p> <p>As an alternative estimation method of thermohydraulic loads in condensation pools, the SILA code based on potential flow theory, was taken into use. SILA solves the pressure distribution caused by oscillating bubbles in a pool, and is easier to use and more flexible than Method Of Images studied earlier. SILA has been modified for pools without an inner cylinder and test simulations for the POOLEX water pool were performed.</p> <p>The MpCCI FSI coupling software employs an explicit coupling scheme, which results in numerical instability in the case of the POOLEX facility. In order to improve stability, ways for implementing an implicit coupling scheme with MpCCI were examined. It was found that such a scheme is difficult to achieve without access to the source codes. An implicit coupling scheme is expected to be available with MpCCI in forthcoming years.</p> <p>A method was developed which can be used for analysing two-way FSI problems realistically by using only one-way coupling of CFD and structural analysis codes. In the method, the mass of the fluid is accounted for in the structural motion by adding the fluid to the structural model as an acoustic medium. Validity of the method was examined with promising results mathematically by an order of magnitude analysis and by comparing numerical results with a full two-way calculation in a simple test case and with a POOLEX experiment. The method has certain restrictions, the most important being that structural displacements have to be sufficiently small. These restrictions do not seem to be too limiting for modeling the POOLEX facility or a real pressure suppression pool. The method may have significance in many other applications as well where structural motion is small but the added mass effect of fluid is significant.</p>	
Confidentiality	Public
Espoo 26.3.2007 Signatures <div style="display: flex; justify-content: space-around; align-items: flex-end;"> <div style="text-align: center;">               Eila Lehmus              Technology Manager         </div> <div style="text-align: center;">               Antti Timperi              Research Scientist         </div> </div>	
VTT's contact address P.O. Box 1000, FI-02044 VTT	
Distribution (customer and VTT) STUK (4), Patrick Isaksson (NKS), Heikki Sjövall (TVO), Olli Nevander (TVO), Markku Puustinen (LUT), Heikki Purhonen (LUT), Arja Saarenheimo (VTT), Antti Timperi (VTT), Timo Pättikangas (VTT), Mikko Ilvonen (VTT), VTT archive	
<i>The use of the name of the Technical Research Centre of Finland (VTT) in advertising or publication in part of this report is only permissible with written authorisation from the Technical Research Centre of Finland.</i>	

## Preface

This study is part of the INTELI (Integrity and Life Time of Reactor Circuits) project carried out in the SAFIR Programme, the Finnish Research Programme on Nuclear Power Plant Safety. This study is partly funded by the State Nuclear Waste Management Fund (VYR) and by the Nordic Nuclear Safety Research (NKS). The contact person in STUK is Dr. Martti Vilpas.

The authors are grateful to the members of the POOLEX project at the Lappeenranta University of Technology, Mr. Markku Puustinen, Mr. Heikki Purhonen and Mr. Antti Räsänen, for providing experimental results.

Espoo 26.3.2007

Authors

# Contents

Nomenclature	4
1 Introduction	6
2 Alternative Methods for the Estimation of Thermohydraulic Loads	7
3 CFD Modelling of Interface Mass Transfer	9
3.1 Simple Model for Direct-Contact Condensation	9
3.2 VOF Simulations of Direct-Contact Condensation	10
3.3 Combining Condensation Model with the FSI Model	19
4 Fluid-structure Calculations with Star-CD and ABAQUS	20
4.1 Two-Way Coupling	20
4.2 One-Way Coupling with Added Mass	21
4.2.1 Description of the Acoustic-Structural Analysis	22
4.2.2 Analysis of the Method	23
4.2.3 Comparison with Two-Way Coupling	30
4.2.4 Comparison with POOLEX Experiment	32
5 Summary and Conclusions	39
References	40

## Nomenclature

### Latin letters

$c$	speed of sound
$C$	specific heat
$d$	diameter
$\mathbf{f}$	force vector
$g$	acceleration of gravity
$\mathbf{g}$	gravity vector
$h$	heat transfer coefficient, specific enthalpy
$H$	volumetric heat transfer coefficient
$I$	turbulence intensity
$\mathbf{I}$	identity tensor
$k$	thermal conductivity, turbulence kinetic energy, iteration step
$K$	bulk modulus
$L$	length
$\dot{m}$	mass flow rate
$n$	time step
$\mathbf{n}$	unit normal vector
$p$	pressure
$Q$	volumetric heat addition rate
$r$	radial coordinate
$Re$	Reynolds number
$s$	source density
$St$	Stanton number
$t$	time
$T$	temperature
$\mathbf{T}$	viscous stress tensor
$\mathbf{u}$	displacement vector
$U$	velocity magnitude
$V$	volume, velocity magnitude
$\mathbf{V}$	velocity vector
$w$	wall displacement
$\mathbf{x}$	position vector
$z$	axial coordinate

### Greek letters

$\phi$	angular coordinate
$\mu$	molecular viscosity
$\lambda$	bulk viscosity
$\rho$	density
$\Gamma$	volumetric mass transfer rate
$\Pi$	dimensionless parameter
$\Omega$	fluid domain

**Subscripts**

<i>ave</i>	average
<i>b</i>	bubble
<i>f</i>	fluid
<i>g</i>	gas
<i>hyd</i>	hydrostatic
<i>i</i>	interface
<i>l</i>	liquid
<i>p</i>	pressure
<i>s</i>	steam
<i>sat</i>	saturated
<i>t</i>	turbulence
<i>w</i>	wall
1	flow with rigid walls
2	flow due to wall flexure

**Superscripts**

<i>i</i>	initial reference magnitude
0	reference magnitude



# 1 Introduction

During a loss-of-coolant accident (LOCA) in boiling water reactors (BWR), a large amount of non-condensable gas and steam would be injected into the pressure suppression pool. Predicting loads on the pool structures in case of such an event is of great importance, but these loads are difficult to model and different phenomena occurring during the event are not well understood. These phenomena include for example bubble dynamics, condensation of steam through different condensation modes and fluid-structure interaction (FSI).

In the POOLEX project of the Finnish Research Programme on Nuclear Power Plant Safety (SAFIR), injection of air and steam into a water pool has been investigated experimentally at Lappeenranta University of Technology. In the first experimental series, air was injected into the pool through a vertical pipe submerged in water (Laine, 2002). In the later series, various experiments with steam have been conducted (Laine and Puustinen, 2004; Laine and Puustinen, 2005; Laine and Puustinen, 2006).

Several different alternatives for modelling two-phase flow of water and steam exist. The simplest approach is the so-called homogeneous two-phase model, where single-phase equations for homogenised mixture of water and steam are solved. No transport equation is solved for the void fraction but it is determined by assuming equilibrium conditions and using the local enthalpy and pressure. Previously, the homogeneous two-phase model was implemented into the commercial Star-CD computational fluid dynamics (CFD) code (Pättikangas et al., 2005). The implementation could not, however, be made numerically robust in transient calculations because of certain properties of the solver (Timperi et al., 2006).

The Volume Of Fluid (VOF) model is another alternative for modelling two-phase flows of water and steam. In the VOF model, an equation for the void fraction is solved in addition to the single-phase momentum and energy equations. The void fraction equation is used for tracking the interface between the phases. Therefore, the VOF model is suitable for modelling large steam bubbles but cannot be used for bubbles smaller than the numerical grid. In earlier studies, the VOF model has been found to be suitable for modelling experiments, where air is blown into a water pool.

Third alternative for modelling water and steam is the Euler-Euler multiphase model, where void fraction, momentum and energy equations are solved for both phases. In Euler-Euler models, it is usually assumed that one of the phases is continuous and the other one is dispersed. The continuous phase can be, for instance, water or steam and the dispersed phase can be bubbles or droplets. It is assumed that one grid cell of the numerical mesh contains a large amount of droplets or bubbles. Therefore, the Euler-Euler model is usually used for small droplets or bubbles where detailed tracking of the interface between the phases is not necessary.

The homogeneous two-phase model is computationally least expensive of the three different alternatives because essentially equations for single-phase flow are solved. In the VOF model, the additional equation for the void fraction increases computing time. The Euler-Euler model is the most CPU time consuming alternative because full equations for both phases are used. In this work, modelling of condensation by using the VOF model is investigated.

Previously, one-way and two-way coupled FSI calculations of the pool have been performed. In the one-way coupled calculations, the pool walls were rigid during the CFD analysis and only fluid pressure was transferred to the structural model (Calonius et al., 2003; Timperi et al., 2004). In the two-way coupled calculations, the motion of the walls was taken into account in the CFD analysis by transferring the structural displacements to the CFD model (Pättikangas et al., 2005; Timperi et al., 2006). The Fluent and Star-CD CFD codes have been used on the fluid side and the ABAQUS finite element method (FEM) code on the structural side. For FSI coupling, commercial coupling tools ES-FSI and MpCCI have been used. In Timperi et al. (2006), two-way FSI calculations were also performed by modeling the pool water as an acoustic medium with ABAQUS. Two-way FSI has been analysed also in the MULTIPHYSICS project of the SAFIR programme, where a large-break loss-of-coolant accident (LBLOCA) has been analysed in a pressurised-water reactor (Timperi et al., 2005). The two-way coupled CFD-FEM calculations of the pool have been numerically unstable, which is due to simple explicit coupling scheme of the available coupling tools.

In Section 2, we discuss estimation of the pressure loads by using the potential flow theory. In Section 3, the modeling of direct contact condensation of steam in CFD calculations is discussed and results of test simulations are presented. In Section 4, different alternatives for improving the numerical stability of two-way fluid-structure coupling are discussed and tested. Finally, Section 5 contains a summary and discussion on the results.

## 2 Alternative Methods for the Estimation of Thermohydraulic Loads

In the following, solution methods alternative to CFD are studied for obtaining estimates for the pressure loads in condensation pool. In addition to CFD, at least two different methods for estimating the pressure loads can be used: potential theory (Giencke, 1981) or acoustic model (Björndahl & Andersson, 1998). In both approaches, experimental information is needed in order to obtain a reliable estimate for the pressure source that is causing wall loads. In the following, solving the loads from potential theory is discussed.

In potential flow theory, the basic equation to be solved is:

$$\nabla^2 p = -s_p \quad (1)$$

where  $s_p$  is the pressure source density. The source term is caused by the changing volume of the bubble at the outlet of the blowdown pipe

$$S_p = \int s_p dV = \rho_f \frac{dV_b}{dt} \quad (2)$$

where  $\rho_f$  is the fluid density,  $V_b$  is the volume of the air or steam bubble and dot stands for time derivative. Therefore, the pressure source is proportional to the second time derivative of the bubble volume.

The pressure source can be determined from experimental results. In principle, an estimate for the bubble volume can be obtained from experimental data. The second time derivative of the bubble volume is needed, which leads to large uncertainties because of the inaccuracies in determining the derivative. An alternative method is backward calculation of the pressure source from experimentally measured pressure loads on the wall. A third possible method is

using divergence theorem and measurement of the pressure gradient near the water surface (see Timperi et al., 2006).

Previously, the use of the Method Of Images (MOI) was studied for solving Eq. (1) for the potential flow (Pättikangas et al., 2005). Another possibility is direct numerical solution of Eq. (1) by using conventional difference methods. These two alternative solution methods were compared in Timperi et al. (2006) and the difference method was chosen.

The SILA programme earlier developed at VTT (Eerikäinen, 1997) has now been taken into use for solving Eq. (1). Previously, SILA has only been applied to annular geometries typical of BWR condensation pools. Therefore, SILA had to be modified for the POOLEX geometry, that is, for cylindrical geometries without any annulus.

Test calculations by using SILA were performed for the POOLEX geometry. In the test simulations, the pressure source was  $S_p = 1$  bar m. The source was located just below the blowdown pipe. The distance of the pressure source from the pool bottom was  $z = 0.7$  m, the distance from the pool axis was  $r = 0.3$  m and the angular coordinate was  $\phi = 315^\circ$ .

The pressure on the pool wall obtained in SILA test simulation is shown in Fig. 1. The pressure load has maximum value in the direction  $\phi = 315^\circ$ , where the pressure source is closest to the pool wall. The pressure load caused by the deforming bubble is largest close to the pool bottom and decreases to zero at the water surface.

The maximum value of the wall load for the pressure source of  $S_p = 1$  bar m was about  $p = 0.5$  bar. Since the Poisson equation for the pressure is linear, the results for other magnitudes of the pressure sources located at the same place can be obtained from the present result by linear scaling of the result.

Wall pressure (bar)

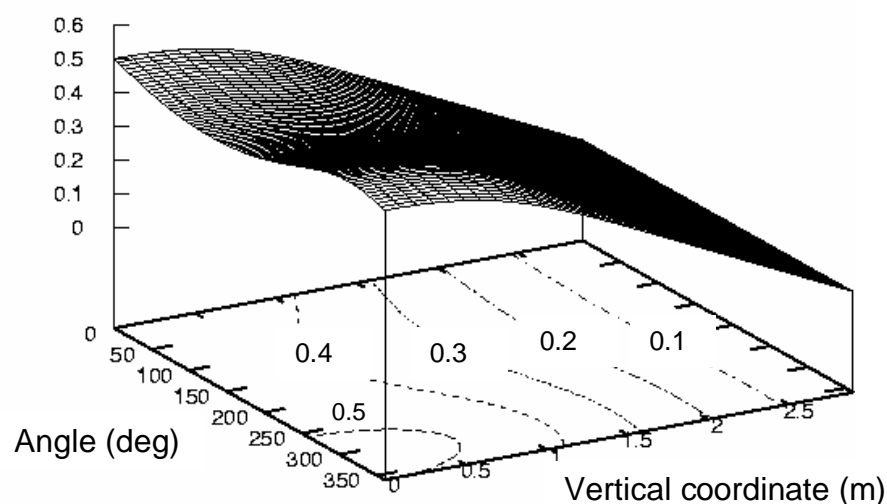


Figure 1. Pressure on the side wall of the water pool. Pressure source of 1 bar m below the blowdown pipe was assumed.

### 3 CFD Modelling of Interface Mass Transfer

In the following, a simple direct-contact condensation model for Volume Of Fluid (VOF) model is described. The model has been implemented in the commercial Fluent CFD code and test simulations have been performed.

#### 3.1 Simple Model for Direct-Contact Condensation

In multiphase models of Fluent CFD code, it is enough to define the mass transfer between the phases. The effect of mass transfer on the energy and momentum equations is taken into account automatically by Fluent. In the following, a simple model for mass transfer in condensation (evaporation) is presented, which has been adapted from approaches used in one-dimensional system codes.

The mass transfer is determined from the energy balance on the interface between the phases (Relap5, 1995)

$$\Gamma_{ig} = -\frac{Q_{ig} + Q_{il}}{h_{g,sat}(p_s) - h_{l,sat}(p_s)} \quad (3)$$

where  $Q_{ig}$  and  $Q_{il}$  are the volumetric heat addition rates ( $\text{W/m}^3$ ) from the gas phase and liquid phase to the interface between the phases. The specific enthalpies ( $\text{J/kg}$ ) for the gas and liquid phases are denoted by  $h_{g,sat}$  and  $h_{l,sat}$ , respectively.

The volumetric heat addition rates are

$$\begin{aligned} Q_{ig} &= \frac{p_s}{p} H_{ig} (T_{sat}(p_s) - T_g) \\ Q_{il} &= H_{il} (T_{sat}(p_s) - T_l) \end{aligned} \quad (4)$$

where  $H_{ig}$  and  $H_{il}$  are volumetric heat transfer coefficients ( $\text{W/Km}^3$ ) from gas and from liquid to the interface, respectively. Here, we assume that the steam does not contain any non-condensable gas and the partial pressure of steam is  $p_s = p$ .

The volumetric heat transfer coefficients are calculated by applying the models of Relap5 for bubbly flow into water pool and into large steam bubbles in the pool. The heat transfer coefficients  $h_{ig}$  and  $h_{il}$  ( $\text{W/m}^2\text{K}$ ) are then calculated from the volumetric heat transfer coefficients and used locally in the VOF calculations.

For water at temperature  $T_l > T_{sat}$ , the heat transfer coefficient is calculated by using the Plesset-Zwick and the modified Lee-Ryley correlations:  $h_{il} = \max\{\text{Plesset-Zwick, Modified Lee-Ryley}\}$ . The heat transfer coefficient is

$$\begin{aligned} h_{il} &= \max \left\{ -\frac{k_l}{d_b} \frac{12}{\pi} \Delta T_{sl} \frac{\rho_l C_{pl}}{\rho_g h_{lg}}, \frac{k_l}{d_b} (2.0 + 0.74 \sqrt{\text{Re}_b}) \right\} \\ \Delta T_{sl} &= T_{sat} - T_l \\ \text{Re}_b &= \frac{(1 - \alpha_b) \rho_l U_{lg} d_b}{\mu_l} \end{aligned} \quad (5)$$

Assuming typical parameters,  $d_b = 0.2$  m,  $k_l = 0.68$  W/mK,  $\Delta T_{sl} = -80$  K,  $\rho_l = 960$  kg/m<sup>3</sup>,  $C_{pl} = 4215$  J/kgK,  $\rho_g = 1...2$  kg/m<sup>3</sup> and  $h_{lg} = 2.2$  MJ/kg, the Plesset-Zwick correlation yields the

result  $h_{il} = 1000...1900 \text{ W/m}^2\text{K}$ . The result depends quite strongly on the steam density (pressure). Assuming that  $\alpha_b \approx 0$ ,  $U_{gl} \approx 0.2...0.5 \text{ m/s}$  and  $\mu_l = 0.28 \times 10^{-3} \text{ Pa s}$ , the Lee–Ryley correlation yields  $h_{il} = 1300...2000 \text{ W/m}^2\text{K}$ .

For water at temperature  $T_l < T_{sat}$ , the Unal & Lahey correlation for the heat transfer coefficient was used. When the heat transfer coefficient is written in terms of the volumetric heat transfer coefficient, we find

$$h_{il} = H_{il} \frac{V}{A_i} = H_{il} \frac{d_b}{6\alpha_b} \quad (6)$$

The Unal & Lahey correlation in simplified form reads

$$h_{il} = \frac{0.075 h_{lg} \rho_g \rho_l}{\rho_l - \rho_g} \frac{d_b}{6} \quad (7)$$

where we have assumed  $F_3 = 1$  and  $F_5 = 0.075$  for the coefficients of the model. Using the typical numerical values given above, we find  $h_{il} = 5500 \text{ W/m}^2\text{K}$ .

An alternative approach is using correlations determined for submerged jets in modelling the heat transfer on the water side of the interface. The available correlations were recently reviewed by Kim et al. (2004). The correlations are based on turbulent fluctuation on the water side which determines the heat transfer. The heat transfer coefficient is

$$h_{il} = \rho_l c_{p,l} I St_t \quad (8)$$

where  $St_t$  is the Stanton number for condensation and  $I = (2k/3)^{1/2} / U_{ave}$  is the turbulence intensity. In the test simulations presented below, the value  $St_t = 0.0131$  was used.

For steam the value  $h_{lg} = 1000 \text{ W/m}^2\text{K}$  was estimated and used both for  $T_g > T_{sat}$  and for  $T_g < T_{sat}$ .

The above formulas in Eqs (5)–(7) have originally been developed for pipe flow, where  $T_l$  and  $T_g$  are the average temperature of the liquid and gas, respectively. In the VOF simulations, the temperatures of the grid cells containing the interface between the phases are used, which are closer to the saturation temperature  $T_{sat}$  than the other grid cells. Therefore, the present approach may underestimate the condensation rate.

In the model described above, the one-dimensional correlations for the bubbly flow regime were applied. Another alternative would be to use the correlations derived for the plug flow, where the flow velocity is perpendicular to the interface between the phases. Third alternative would be the correlations of the stratified flow, where the flow velocity is parallel the interface between the phases. It seems, however, that in these one-dimensional models the pipe wall is implicitly included, which makes modifications to three-dimensional geometries difficult.

### 3.2 VOF Simulations of Direct-Contact Condensation

Test simulations with the direct-contact condensation model described above were performed. The simulations were done with Fluent version 6.3.26, where the above direct-contact condensation model was implemented by using user defined functions of Fluent. The numerical mesh contained about 94 000 hexahedral grid cells. The Volume Of Fluid (VOF) model of Fluent was used with explicit interpolation scheme. Second order upwind method

was used for discretization of density, momentum, turbulence and energy equations. Modified HRIC method was used for the volume fraction. The PRESTO method was used for discretization of pressure and PISO was used for pressure-velocity coupling. Turbulence was modelled with standard  $k-\varepsilon$  model of Fluent by using wall functions. The time step in the simulation was  $\Delta t = 0.5$  ms.

Initially, the water level in the pool was at  $z = 3.08$  m, where the coordinate system is chosen so that the bottom of the pool is at  $z = 0$ . The water temperature was  $T = 40$  °C and the region above the water contained steam with a temperature of  $T = 105$  °C and a pressure of  $p = 1$  bar. The blowdown pipe was initially full of steam at a temperature of  $T = 105$  °C and a pressure of  $p = 1$  bar. The pipe wall above the water level was preheated and the wall temperature was initially  $T_w = 105$  °C. At time  $t = 0$ , valve was opened at the top part of the blowdown pipe and the mass flow rate of steam was set to a constant value of  $\dot{m} = 0.36$  kg/s with a temperature of  $T = 105$  °C.

A result of a test simulation is shown in Fig. 2, where the void fraction is shown at different instants of time. In early stage of the simulation ( $t < 0.5$  s), the wall condensation in the pipe is quite strong at the water level and the pressure in the top part of the pipe decreases. The water in the pipe moves first slightly upwards but starts then accelerating downwards. At time  $t = 0.785$  s, the water plug is expelled from the pipe. At this time, the velocity of the water plug is about 11.6 m/s.

The steam jet following the accelerated water plug hits the bottom of the pool at time  $t = 0.9$  s. The front edge is then condensed and the jet has become shorter at time  $t = 1.15$  s. After that the steam bubble oscillates back and forth at the pipe outlet. The bubble becomes longer again at time  $t = 1.40, 1.55$  and  $1.70$  s. The period of this back and forth motion is about  $\Delta t = 0.15 \dots 0.2$  s.

In Fig. 3, the temperature of the water-steam mixture and the mass transfer rate between the phases is shown at different instants of time. At time  $t = 0.90$  s, hot steam jet hits the pool bottom and the temperature at the pool bottom reaches for a while the value 100 °C. At time  $t = 1.80$  s, the oscillating steam bubble has moved upwards and the temperature at the pool bottom decreases to about 70 °C. The maximum rate of mass transfer from steam to water phase is about 24 kg/m<sup>3</sup>s. The condensation occurs within a small region around the oscillating steam bubble. Small amount of evaporation also occurs in regions where small amount of water is in contact with large amounts of steam. The maximum evaporation rate is about 0.2...0.3 kg/m<sup>3</sup>s.

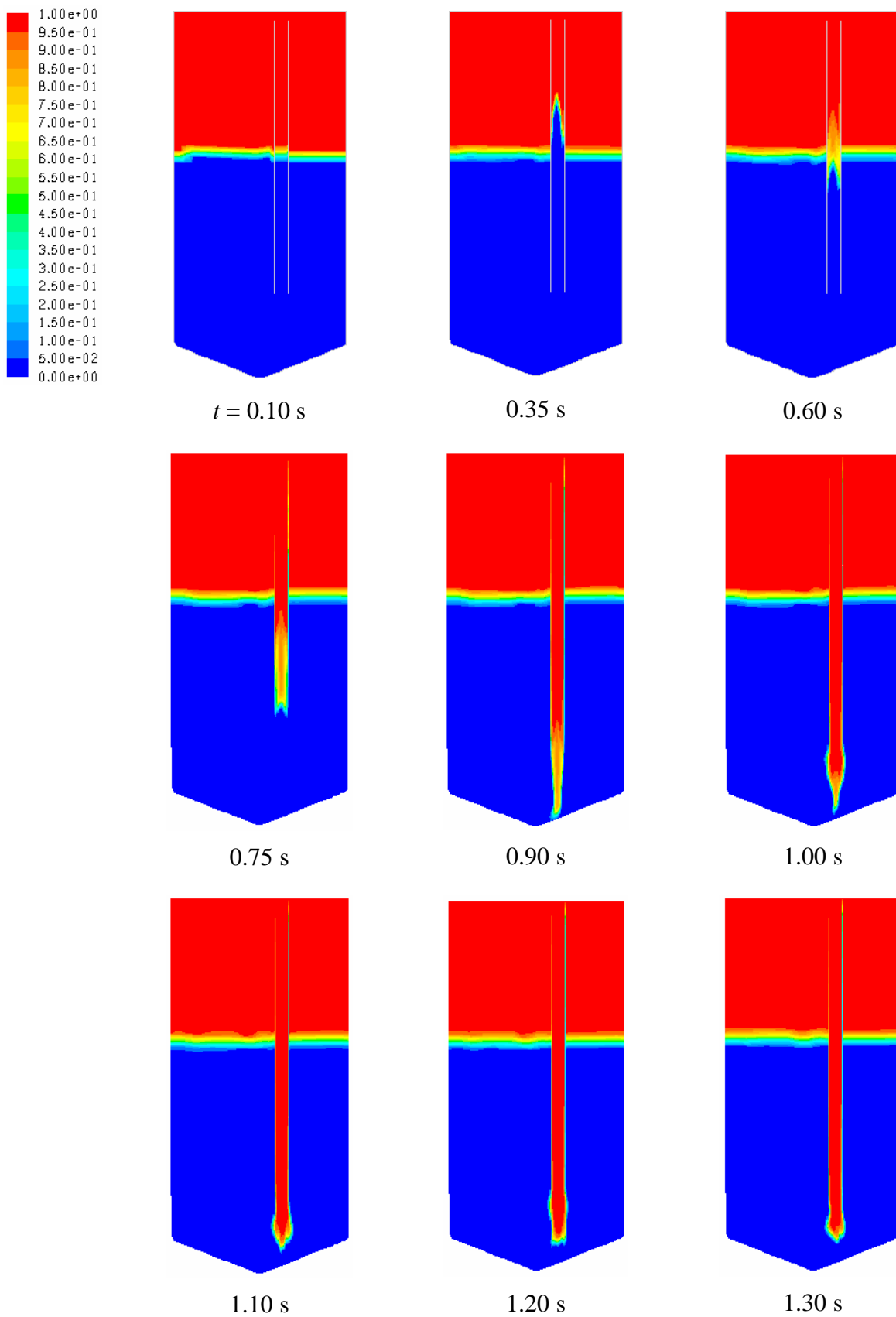


Figure 2. Void fraction at different instants of time, when steam is blown into the water pool. The mass flow rate of steam is  $\dot{m} = 0.36$  kg/s and the temperature of the pool is  $40^\circ\text{C}$  (continues on the following pages).

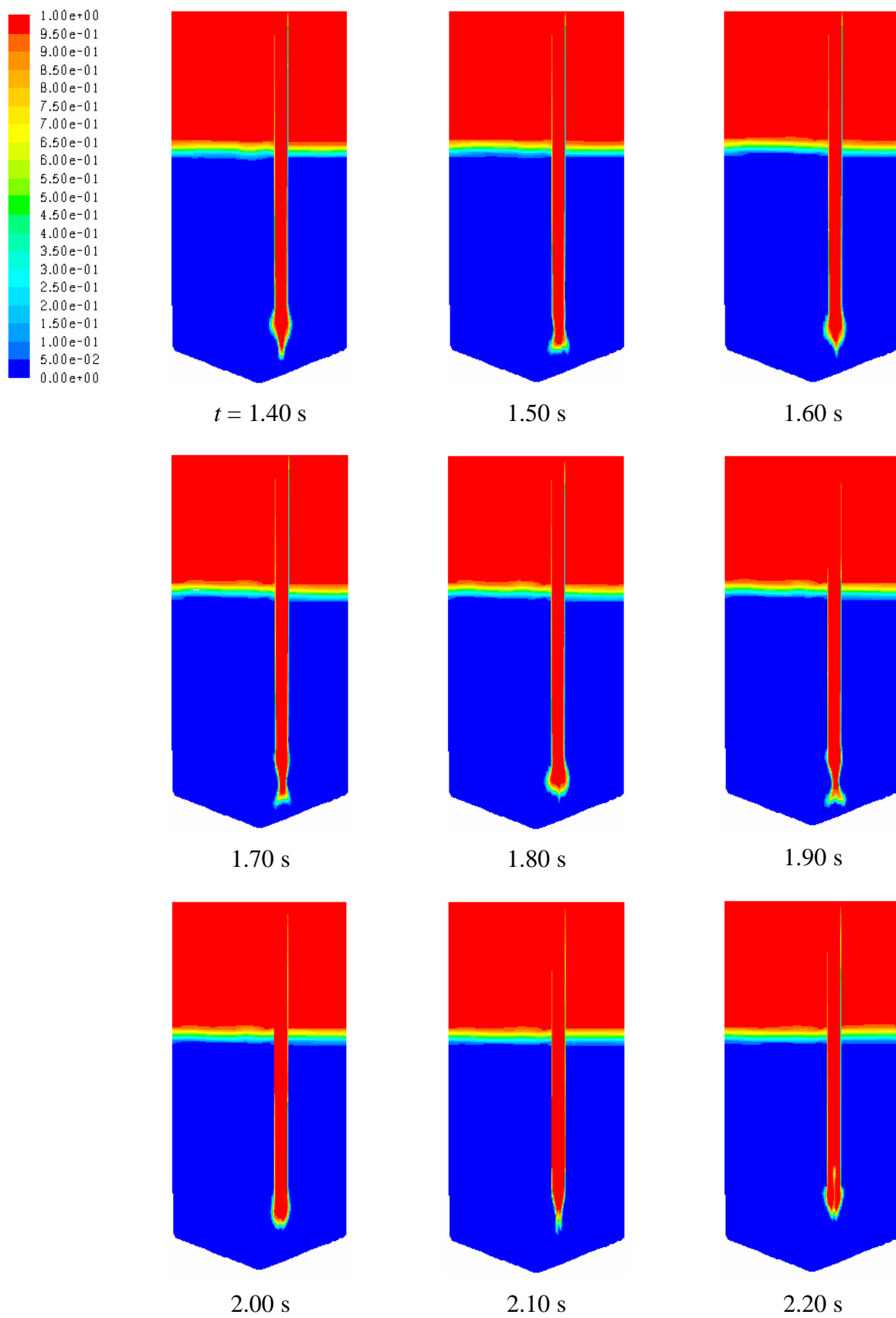


Figure 2. Continues from the previous page.



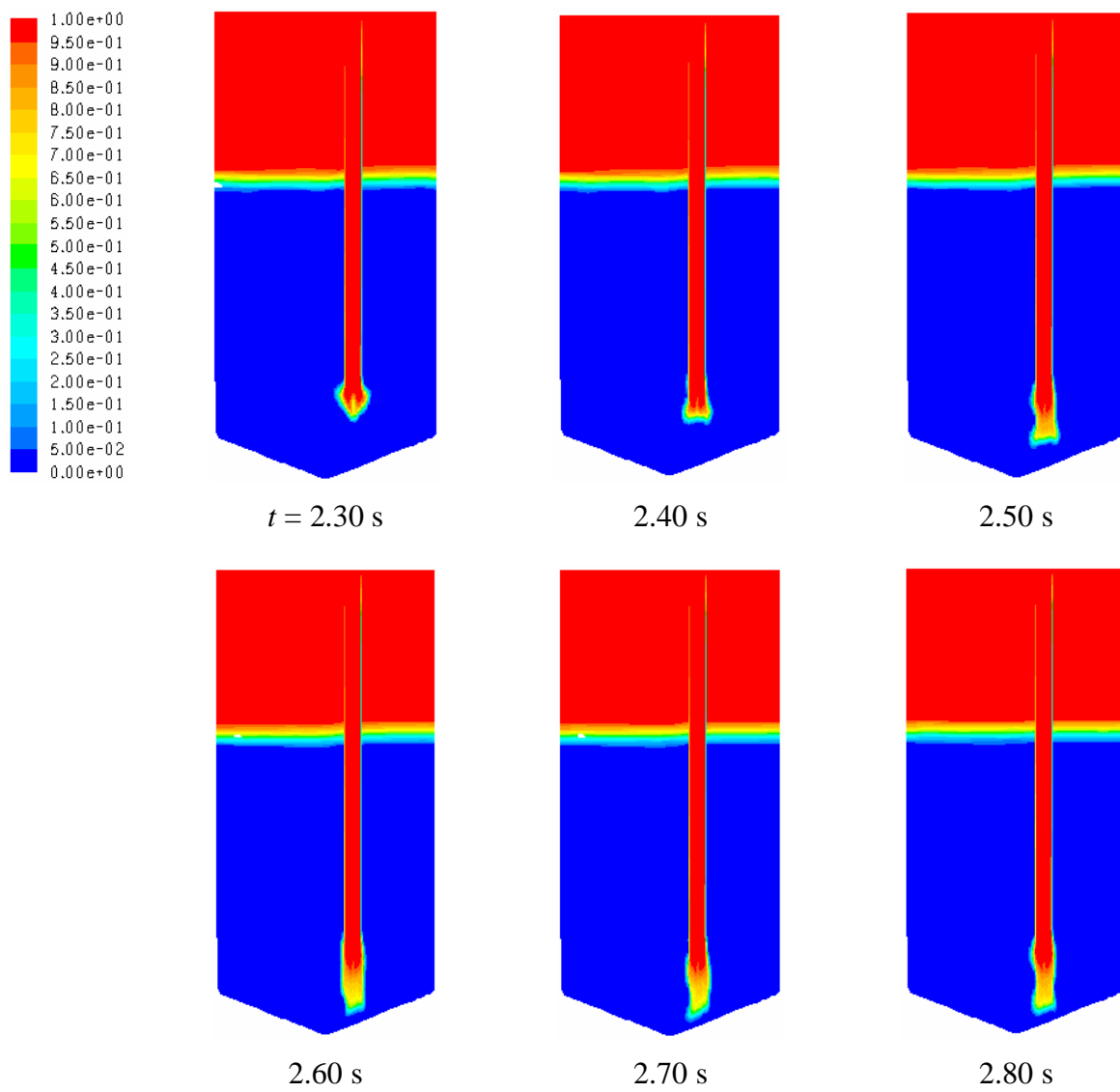


Figure 2. Continues from the previous pages.

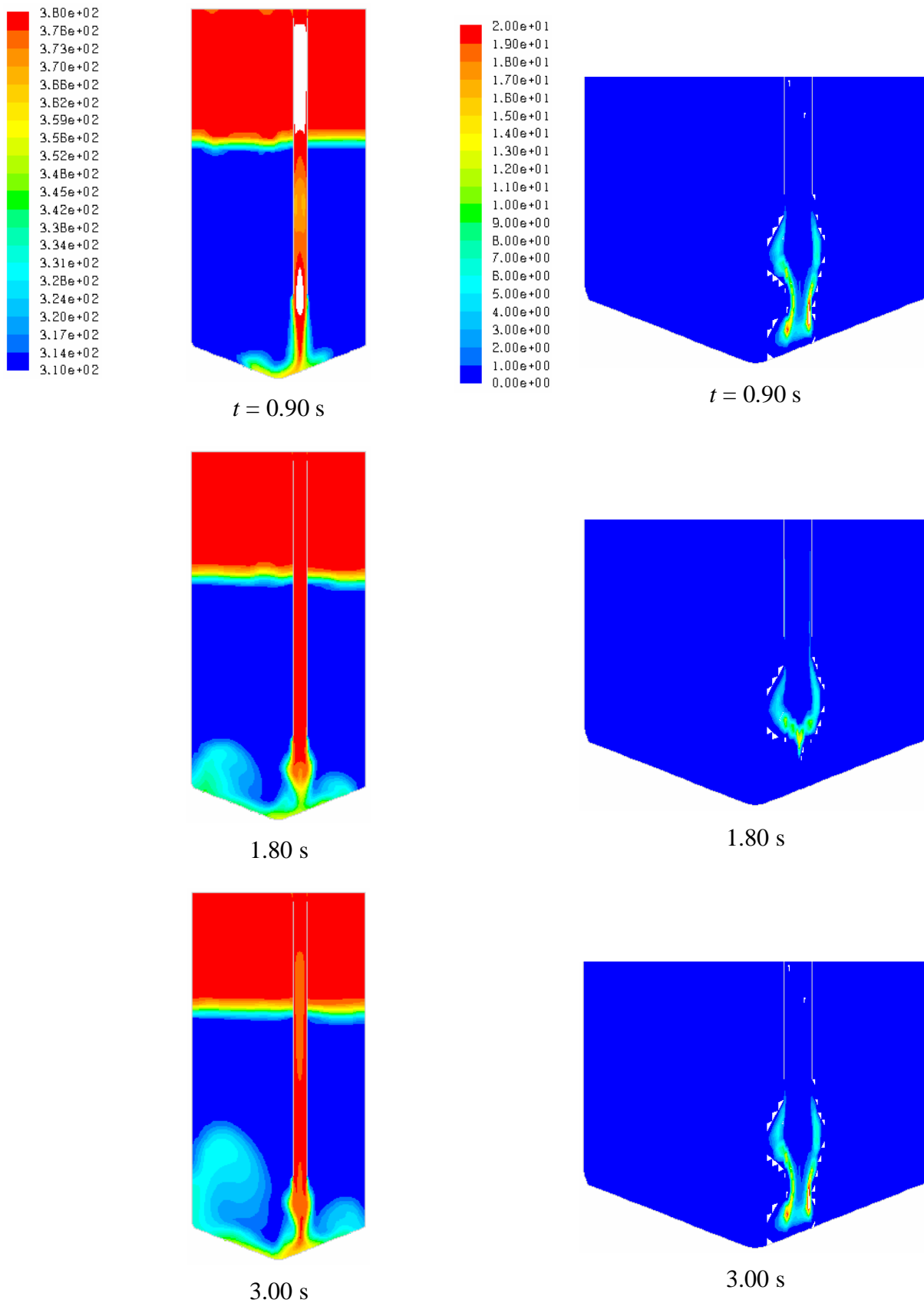


Figure 3. Temperature (K) of the water-steam mixture (left) and mass transfer rate (kg/m<sup>3</sup>s) between the phases (right) at different instants of time. The mass flow rate of steam in the pipe is  $\dot{m} = 0.36$  kg/s and the temperature of the pool is initially  $T = 40$  °C.

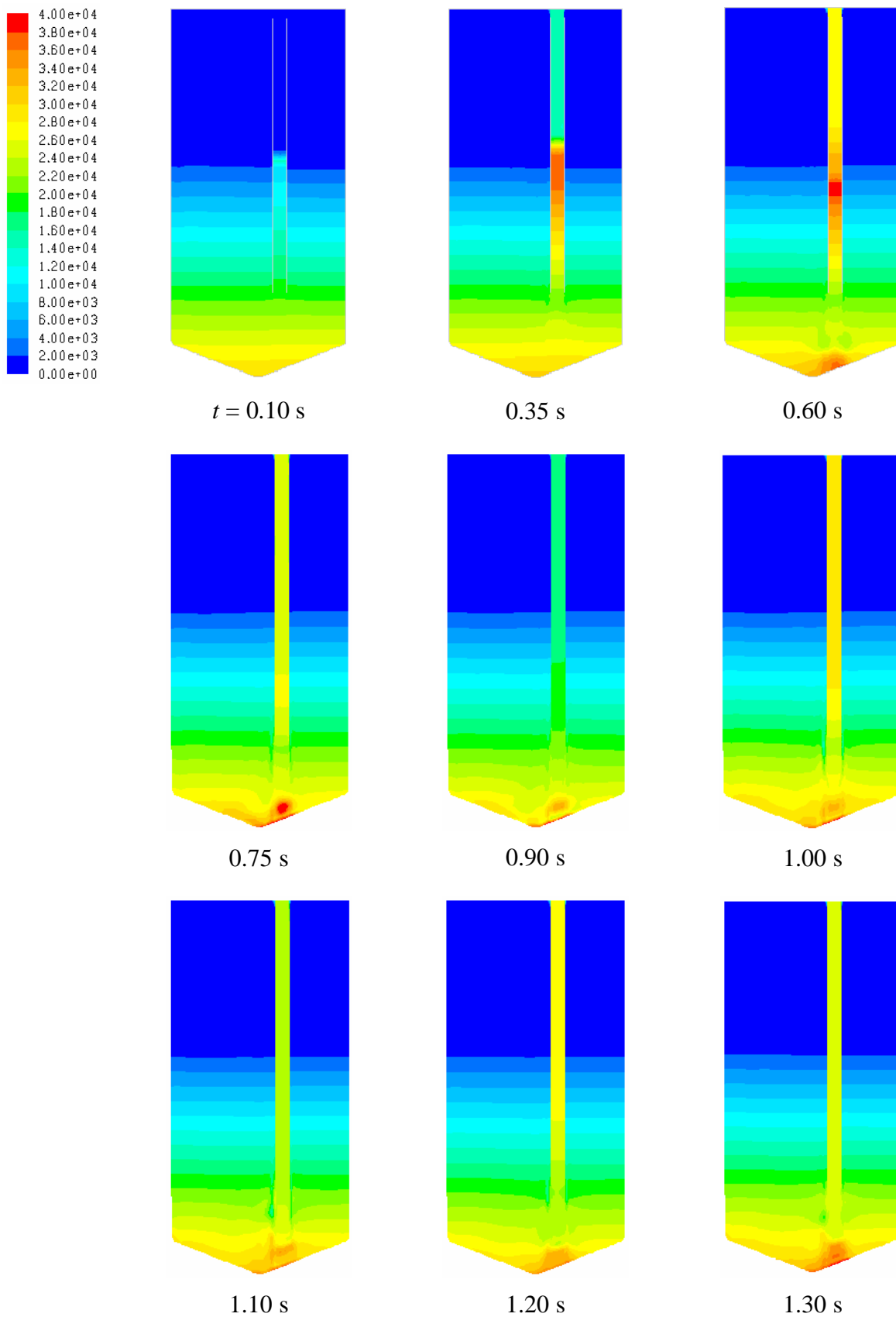


Figure 4. Static relative pressure (Pa) in the pool at different instants of time. The mass flow rate of steam is  $\dot{m} = 0.36$  kg/s and the temperature of the pool is 40 °C (continues on the following pages).

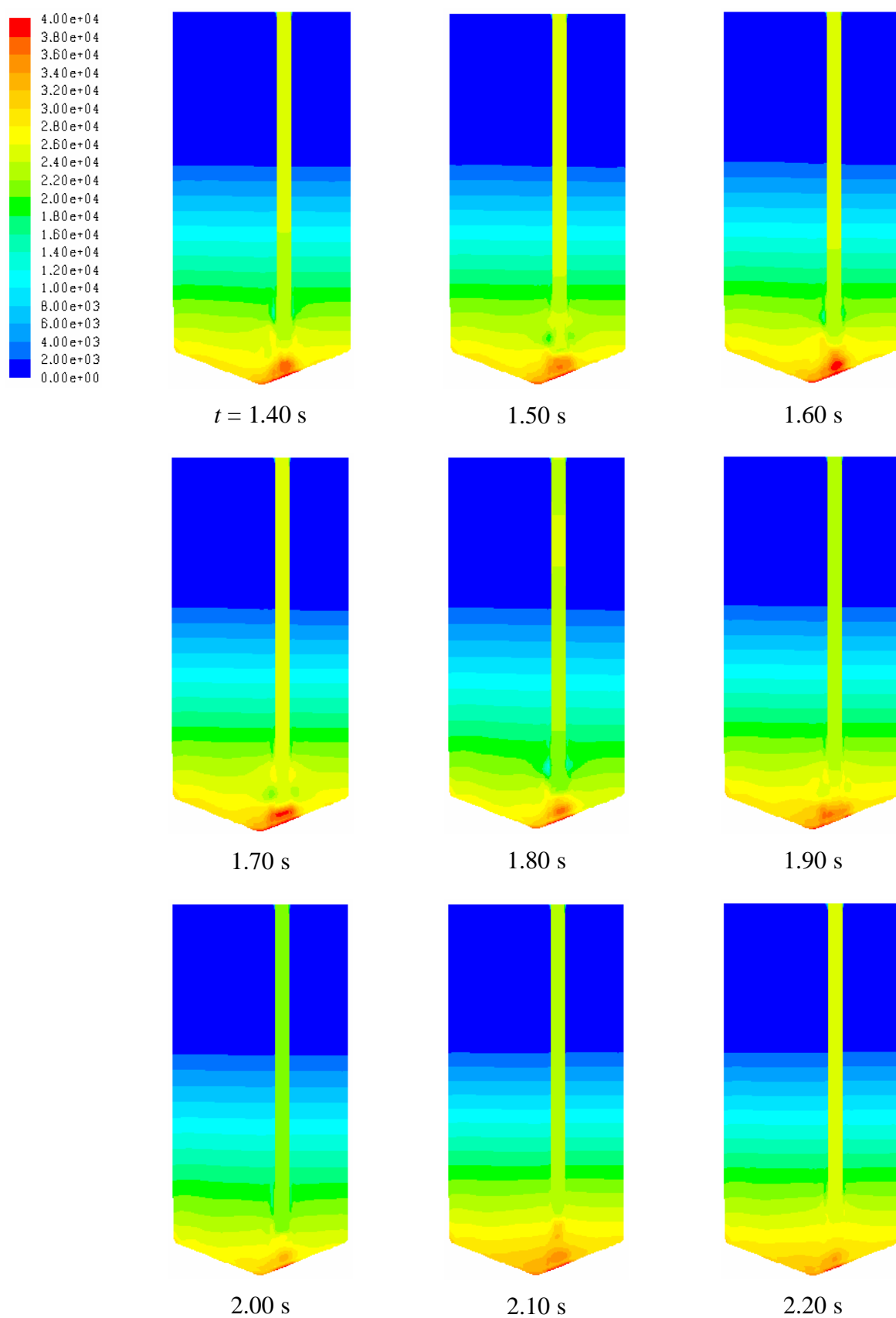


Figure 4. Continues from the previous page.

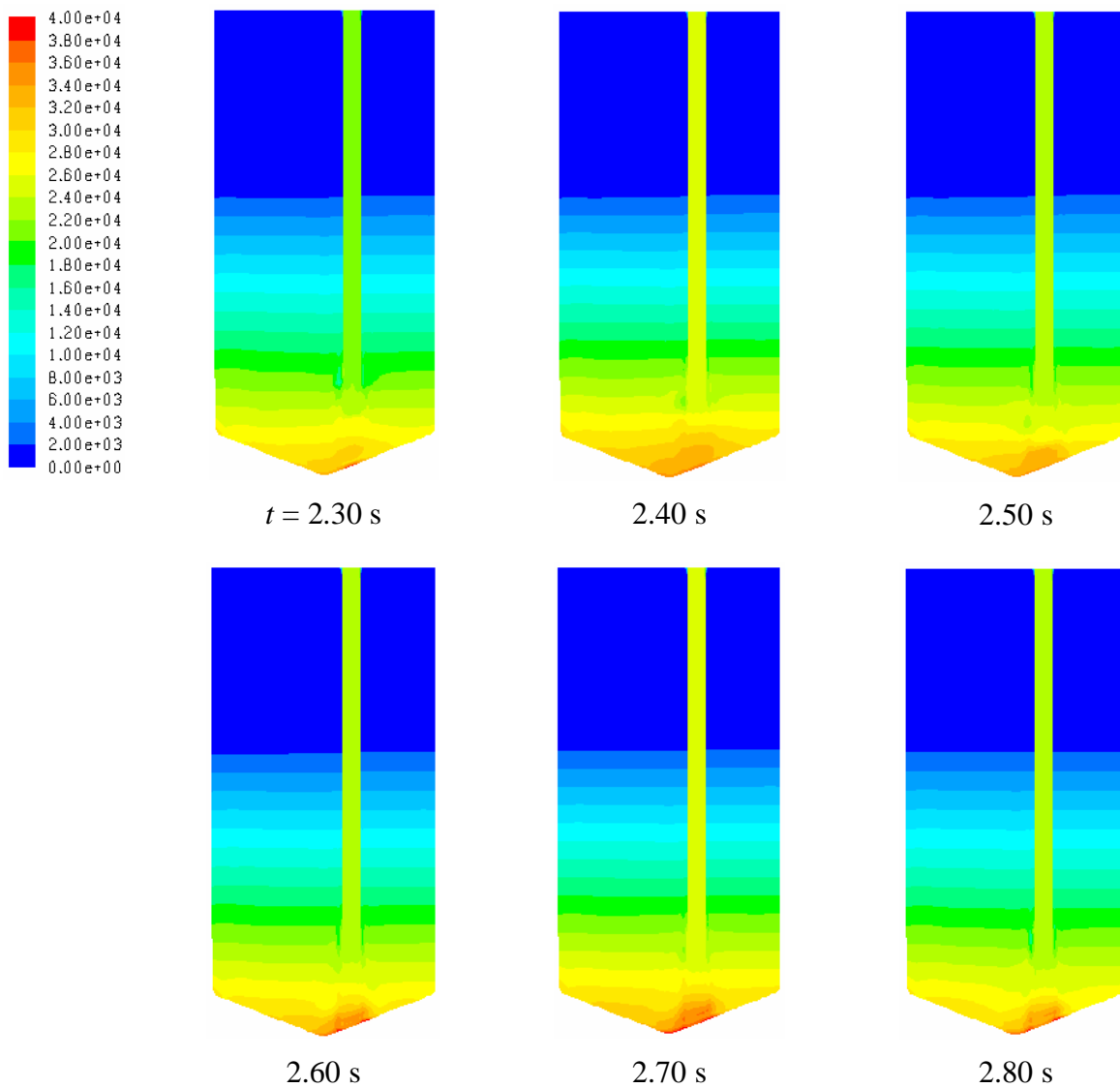


Figure 4. Continues from the previous pages.

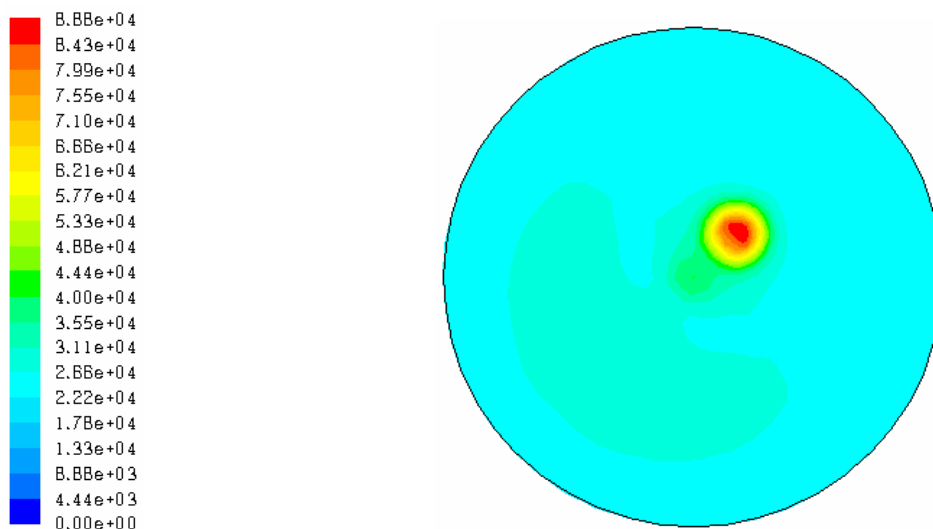


Figure 5. Static relative pressure load (Pa) on the pool bottom at time  $t = 0.85$  s.

In Fig. 4, pressure in the water pool is shown at different instants of time. The hydrostatic pressure at the pool bottom ( $z = 0$ ) is initially  $p_{hyd} = 30$  kPa corresponding to the initial water level of  $z = 3.08$  m. The pressure load on the pool bottom increases, when the water plug is accelerated in the blowdown pipe in the time interval  $t = 0 \dots 0.85$  s. Thereafter, the pressure oscillates, when the bubble size grows and decreases at the pipe outlet.

The maximum pressure load on the pool bottom occurs at time  $t = 0.85$  s (see Fig. 5). The maximum load is located directly below the blowdown pipe and it is caused by the accelerating water plug. The maximum load is  $p_w = 89$  kPa, which is 59 kPa above the hydrostatic pressure at the pool bottom.

The parameters of the simulation described above correspond to the POOLEX experiment STB-14-2. The numerical results obtained have clear differences compared to the experimental result. The condensation rate of steam is too small and the interface of steam and water remains outside of the pipe all the time during the simulation. In the experiment, chugging occurs as is expected and the interface between the phases moves periodically into the blowdown pipe when rapid condensation of a steam bubble occurs. A possible reason for this is a rapid increase of the interface area between steam and water, which rapidly increases heat transfer and condensation.

The calculated shape of the bubble differs from the one observed in the experiments. In vertical direction, the calculated diameter of the bubble is too large. In the horizontal direction, the calculated diameter is too small. Therefore, improvements of the numerical model must affect the heat transfer in anisotropic manner around the bubble. Heat transfer should be larger below the bubble and smaller in other directions.

### 3.3 Combining Condensation Model with the FSI Model

In calculations of fluid-structure interactions, the Massively parallel Code Coupling Interface (MpCCI) library developed at the Fraunhofer Institute was used for coupling Fluent with ABAQUS. MpCCI performs interpolation between the different numerical meshes of the CFD and structural analysis codes, when data on pressure loads and wall positions are exchanged between the codes.

Fluent implementation of the MpCCI library uses User Defined Functions of the Fluent code. Since the condensation model described in Section 3.1 also uses User Defined Functions of the Fluent code, some conflicts between MpCCI and Fluent 6.2 occurred. In Fluent 6.2, it was necessary to modify the MpCCI library routines by adding calls to the subroutines of the condensation model. Fluent 6.3.26 released in December 2006, however, contained a significant improvement, which makes it possible to link several subroutine libraries in a flexible manner. Therefore, Fluent 6.3.26 was finally used in combined test calculations, where both the condensation model and fluid-structure interaction were simultaneously tested.

## 4 Fluid-structure Calculations with Star-CD and ABAQUS

Fluid-structure interaction calculations carried out with Star-CD and ABAQUS are described in the following. The external coupling software MpCCI was used for one-way and two-way coupling of the fluid and structure codes. In the earlier work (Pättikangas et al., 2005; Timperi et al., 2006), the internal coupling tool ES-FSI of Star-CD was used. MpCCI is an improvement over ES-FSI as the memory requirement with large structural models is far less (see Pättikangas et al., 2005) and nearly full capabilities of the coupled codes, e.g. using a non-linear structural model, are allowed.

One particular advantage of using Star-CD instead of Fluent in FSI calculations with MpCCI, at least with current code versions, is that the transfer of nodal displacements instead of absolute coordinates from the structural model is not supported with Fluent as it is with Star-CD. Using the nodal displacements is required when a gap must be allowed between the fluid and structure meshes, which is often the case when using shell elements. Also in most cases it seems more convenient to use displacements since then artificial pressure peaks, resulting from adjustment of the meshes during the first few time steps due to slight initial discrepancies between the meshes, is automatically avoided. In addition, it is of interest to use different codes as they usually have their own advances and in-house models developed into them.

### 4.1 Two-Way Coupling

As was discussed in the earlier work (Timperi et al., 2006), the two-way coupled FSI calculations of the pool are numerically unstable when using a simple explicit coupling scheme. MpCCI offers different variations of the explicit scheme according to the timing of data transfer and according to which code is the simulation leader. These variations have slightly different stability characteristics, but according to test calculations they may be of help only in mildly unstable cases. Shortening time step may usually be used for improving stability, but in the case of the pool the instability is so severe that time step would have to be impractically short for simulation times of order 1 second. It is also possible, especially when modeling water as incompressible, that the pool is unconditionally unstable with an explicit scheme, as some FSI cases are (see Causin et al., 2004).

The most important physical parameters influencing stability seem to be the compressibility of the fluid and the ratio of structure density to fluid density. Decreasing either of these parameters will decrease stability (Timperi et al., 2006; Causin et al., 2004; Anon., 2005). For example, air has high compressibility and low density compared to water, which should make air far more tractable in FSI calculations. Stability of an FSI calculation may not be an issue also when pressure wave propagation is modelled, since water is necessarily modelled as compressible and simulation time is usually very short, making short time steps practical.

The main cure that has been presented for the numerical instability is the implicit coupling scheme (Causin et al., 2004; Matthies and Steindorf, 2002; Abouri et al., 2004; Sigrist and Abouri, 2006; Vierendeels et al., 2005). This is an iterative method in contrast to the explicit scheme, where data is exchanged only once between each time step. A flow chart showing an example of explicit and implicit FSI calculations is presented in Fig. 6. As can be seen from

Fig. 6, data is exchanged multiple times during iteration inside time step in the implicit scheme. Underrelaxation is usually used in order to stabilize the iteration (Causin et al., 2004; Vierendeels et al., 2005).

The implicit scheme shown in Fig. 6 is only a slight extension over the explicit one. Possibilities of implementing this kind of scheme with MpCCI were examined but none were found without access to the source codes. The difficulty is that the calculation in both codes would have to be initialised to the converged state of the previous time step after each iteration step. This is because calculation of each time step has to be repeated several times in both codes due to the iteration.

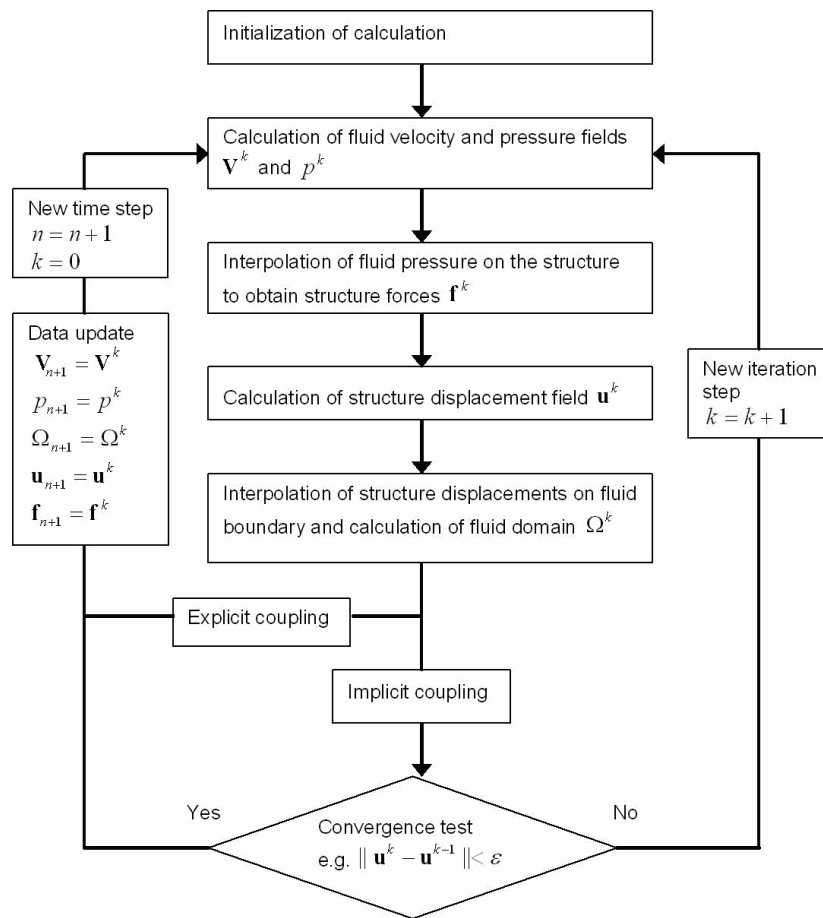


Figure 6. Explicit and implicit fluid-structure coupling (after Causin et al., 2004; Sigrist and Abouri, 2006).

## 4.2 One-Way Coupling with Added Mass

As implementing the implicit scheme with full two-way FSI coupling was found to be untractable, means for performing realistic FSI calculations by using the one-way coupling, in which only the fluid pressure is transferred to the structural model, were searched. A natural point of departure for such a method is that the structural displacements would have to be small so that they would not affect the flow field significantly. This should be the case for many of the loading situations of the POOLEX facility and perhaps even more so for a real pressure suppression pool in which the walls are made of concrete. For example, in the POOLEX experiments the scale of the motion of the gas-water interface is usually at least of



order hundreds of millimeters and the scale of the pool is of order few meters, whereas the maximum deflection of the pool wall is about one millimeter. Surely even small amplitude wall motion can cause significant pressure fluctuations in the water, but this does not necessarily affect the actual fluid flow problem, as is shown later.

Perhaps the main problem with a straightforward one-way coupling, assuming that the structural displacements are negligible for the flow problem, is that the added mass effect of the fluid is not accounted for in the structure. In other words, as the transient fluid pressure is applied on the structure, its frequency of motion is as if the fluid was absent. Obviously if the fluid is light this may not be a problem, but for example in the POOLEX facility the mass of the structure is much less than that of the water. For structures undergoing mainly rigid body motion, such as a beam immersed in a fluid or fluid filled pipe undergoing transverse vibrations, the added mass effect of the fluid can be often accounted for by simply adding an appropriate mass to the structure (see e.g. Moody, 1990). This approach is not, however, suitable for example for the POOLEX facility, where the wall motion is non-uniform.

In the previous work (Timperi et al., 2006), the coupled FSI eigenfrequencies of the pool were calculated by using the two-way coupled acoustic-structural capability of ABAQUS, which accounts for the fluid mass in the structural motion. This procedure was also validated for two simple test cases and it has been used in dynamic direct integration FSI analyses as well (Timperi et al., 2005). In Timperi et al. (2005), good agreement was found with fully coupled CFD-FEM calculations. Since the acoustic part of the ABAQUS model may be included in FSI calculation with MpCCI, the following method is proposed:

- Construct the coupled acoustic-structural ABAQUS model, in which water is modeled as an acoustic medium and in which the pressures and displacements on the fluid-structure interface are coupled.
- Construct the usual CFD model of the fluid problem.
- Perform one-way coupled FSI calculation with MpCCI by transferring only fluid pressure on the fluid-structure interface.

By using this method, the effect of the fluid on the motion of the structure is accounted for. The method has some restrictions in addition to the obvious one of small structural displacements, these are discussed in Sec. 4.2.2. It was found that the basic principle of the method, i.e. solving a multidimensional flow problem due to wall motion separately, is not novel (see Sonin, 1980), but it may be novel with modern commercial codes. The method has significance in that it can be used for solving complex three-dimensional two-way FSI problems as long as certain requirements, which are not very restrictive in many practical cases, are met (see Sec. 4.2.2 later). Essentially the same method has been validated with good results against a small-scale blowdown experiment by Huber et al., (1979).

#### 4.2.1 Description of the Acoustic-Structural Analysis

The coupled acoustic-structural analysis capability of ABAQUS is reviewed shortly in the following. The equations are slightly simplified from those given in ABAQUS (2006). ABAQUS offers elements that can be used to model a compressible fluid medium undergoing small pressure variations. These acoustic elements have pressure as the only degree of freedom. In the coupled acoustic-structural analysis, motions of a solid structure are solved together with the acoustic medium. In this case, the acoustic pressure is applied on the surface of the structure and the motion of the structure creates pressure variations to the acoustic

medium. A variety of boundary conditions are available for the acoustic medium, only two of which are of interest for the present work:

- Prescribed pressure at the boundary nodes (here zero for a free surface).
- Prescribed normal derivative of pressure on the boundary (zero for a rigid wall and proportional to acceleration for a moving wall).

The equilibrium equation for the fluid is described with

$$\nabla p + \rho \mathbf{a} = 0 \quad (9)$$

where  $p$  is the pressure in the fluid in excess of any static pressure,  $\rho$  is the density of the fluid and  $\mathbf{a}$  is the acceleration of the fluid particle. A linear inviscid constitutive behaviour is assumed for the fluid:

$$p = -K \nabla \cdot \mathbf{u} \quad (10)$$

where  $K$  is the bulk modulus of the fluid and  $\mathbf{u}$  is the displacement of the fluid particle. Eq. (10) states that pressure is proportional to volumetric strain, i.e. dilation. By using Eq. (10), the wave equation can be derived from Eq. (9):

$$\mathbf{a} - c^2 \nabla^2 p = 0 \quad (11)$$

where  $c$  is the speed of sound  $c = (K/\rho)^{1/2}$ . On the fluid-structure interface, pressures and displacements normal to the interface are coupled:

$$p_{fluid} = p_{structure} \quad (12)$$

and

$$\mathbf{n} \cdot \mathbf{u}_{fluid} = \mathbf{n} \cdot \mathbf{u}_{structure} \quad (13)$$

where  $\mathbf{n}$  is unit normal vector of the interface. Acceleration of the interface affects the normal derivative of pressure on the acoustic boundary by equation

$$\rho \mathbf{n} \cdot \mathbf{a} = -\mathbf{n} \cdot \nabla p \quad (14)$$

On a rigid boundary, we have  $\mathbf{a} = 0$  and

$$\mathbf{n} \cdot \nabla p = 0 \quad (15)$$

#### 4.2.2 Analysis of the Method

Validity of the proposed calculation method is examined in this chapter with guide lines taken from Sonin (1980). For the water in the pool, we have the conservation equations of mass and momentum for compressible fluid:

$$\frac{\partial \rho}{\partial t} + \nabla \cdot (\rho \mathbf{V}) = 0 \quad (16)$$

$$\rho \left( \frac{\partial \mathbf{V}}{\partial t} + (\mathbf{V} \cdot \nabla) \mathbf{V} \right) = -\nabla p + \nabla \cdot \mathbf{T} + \rho \mathbf{g} \quad (17)$$

where  $\mathbf{T}$  is the viscous stress tensor

$$\mathbf{T} = \mu(\nabla \mathbf{V} + (\nabla \mathbf{V})^T) + \lambda(\nabla \cdot \mathbf{V})\mathbf{I} \quad (18)$$

In the following, constant viscosity and negligible bulk viscosity are assumed which makes the viscous terms linear. The following pressure-density relation is used:

$$\frac{\partial p}{\partial \rho} = c^2 \quad (19)$$

which is assumed to be linear:

$$\frac{\Delta p}{\Delta \rho} = c^2 \quad (20)$$

The variables of the flow solution of the coupled FSI problem are separated into components that would occur if the walls were rigid (1) and to the components resulting from the flexure of the walls (2):

$$\begin{aligned} \mathbf{V}(\mathbf{x}, t) &= \mathbf{V}_1(\mathbf{x}, t) + \mathbf{V}_2(\mathbf{x}, t) \\ p(\mathbf{x}, t) &= p_1(\mathbf{x}, t) + p_2(\mathbf{x}, t) \\ \rho(\mathbf{x}, t) &= \rho_1(\mathbf{x}, t) + \rho_2(\mathbf{x}, t) \end{aligned} \quad (21)$$

Note that in (21) no assumption of linearity has been made, but the variables are merely separated into the above-mentioned components.

For the rigid wall flow, since by definition the components 2 due to wall flexure are zero, we have

$$\frac{\partial \rho_1}{\partial t} + \nabla \cdot (\rho_1 \mathbf{V}_1) = 0 \quad (22)$$

$$\rho_1 \left( \frac{\partial \mathbf{V}_1}{\partial t} + (\mathbf{V}_1 \cdot \nabla) \mathbf{V}_1 \right) = -\nabla p_1 + \nabla \cdot \mathbf{T}_1 + \rho_1 \mathbf{g} \quad (23)$$

Substituting (21) into (16) and (17) and subtracting from the resulting equations the rigid wall equations (22) and (23), respectively, we obtain equations for the solution of the flow field due to wall flexure:

$$\frac{\partial \rho_2}{\partial t} + \mathbf{V}_2 \cdot \nabla \rho_2 + \rho_2 \nabla \cdot \mathbf{V}_2 + \rho_1 \nabla \cdot \mathbf{V}_2 + \rho_2 \nabla \cdot \mathbf{V}_1 + \mathbf{V}_1 \cdot \nabla \rho_2 + \mathbf{V}_2 \cdot \nabla \rho_1 = 0 \quad (24)$$

$$\begin{aligned}
 (\rho_1 + \rho_2) \left( \frac{\partial \mathbf{V}_2}{\partial t} + (\mathbf{V}_2 \cdot \nabla) \mathbf{V}_2 + (\mathbf{V}_1 \cdot \nabla) \mathbf{V}_2 + (\mathbf{V}_2 \cdot \nabla) \mathbf{V}_1 \right) + \\
 \rho_2 \left( \frac{\partial \mathbf{V}_1}{\partial t} + (\mathbf{V}_1 \cdot \nabla) \mathbf{V}_1 \right) = -\nabla p_2 + \nabla \cdot \mathbf{T}_2 + \rho_2 \mathbf{g}
 \end{aligned} \quad (25)$$

Next, we nondimensionalize (24) and (25) in order to examine the relative magnitudes of their terms. Our hope is that we can neglect all terms containing the rigid wall solution components 1 as small from (24) and (25), thus leaving us with uncoupled equations for the rigid wall solution and for the solution due to wall flexure. Then we can solve the problems separately and sum the results afterwards by using (21). The variables are nondimensionalized as follows:

$$\begin{aligned}
 \mathbf{V}_j^* &= \frac{\mathbf{V}_j}{V_j^0} \quad (j=1,2), \quad p_j^* = \frac{p_j}{p_j^0} \quad (j=1,2), \\
 \rho_1^* &= \frac{\rho_1 - \rho^i}{\rho_1^0 - \rho^i} = \frac{\rho_1 - \rho^i}{\Delta \rho_1}, \quad \rho_2^* = \frac{\rho_2}{\rho_2^0}, \\
 t^* &= \frac{t}{t^0}, \quad \nabla^* = L \nabla, \quad \mathbf{g}^* = \frac{\mathbf{g}}{g}
 \end{aligned} \quad (26)$$

Now all dimensionless variables and their derivatives are  $O(1)$  if the reference magnitudes are chosen properly. Substitution of (26) into (24) and (25) gives dimensionless equations

$$\begin{aligned}
 \frac{\rho_2^0}{t^0} \frac{\partial \rho_2^*}{\partial t^*} + \frac{V_2^0 \rho_1^i}{L} \nabla^* \cdot \mathbf{V}_2^* + \frac{V_2^0 \rho_2^0}{L} (\rho_2^* \nabla^* \cdot \mathbf{V}_2^* + \mathbf{V}_2^* \cdot \nabla^* \rho_2^*) + \\
 \frac{V_2^0 \Delta \rho_1}{L} (\rho_1^* \nabla^* \cdot \mathbf{V}_2^* + \mathbf{V}_2^* \cdot \nabla^* \rho_1^*) + \frac{V_1^0 \rho_2^0}{L} (\rho_2^* \nabla^* \cdot \mathbf{V}_1^* + \mathbf{V}_1^* \cdot \nabla^* \rho_2^*) = 0
 \end{aligned} \quad (27)$$

$$\begin{aligned}
 (\rho^i + \Delta \rho_1 \rho_1^* + \rho_2^0 \rho_2^*) \left( \frac{V_2^0}{t^0} \frac{\partial \mathbf{V}_2^*}{\partial t^*} + \frac{V_1^0 V_2^0}{L} ((\mathbf{V}_1^* \cdot \nabla^*) \mathbf{V}_2^* + (\mathbf{V}_2^* \cdot \nabla^*) \mathbf{V}_1^*) + \frac{V_2^{02}}{L} (\mathbf{V}_2^* \cdot \nabla^*) \mathbf{V}_2^* \right) + \\
 \rho_2^* \left( \frac{V_1^0 \rho_2^0}{t^0} \frac{\partial \mathbf{V}_1^*}{\partial t^*} + \frac{V_1^{02} \rho_2^0}{L} (\mathbf{V}_1^* \cdot \nabla^*) \mathbf{V}_1^* \right) = -\frac{p_2^0}{L} \nabla^* p_2^* + \frac{\mu W_2^0}{L^2} \nabla^* \cdot \mathbf{T}_2^* + \rho_2^0 g \rho_2^* \mathbf{g}^*
 \end{aligned} \quad (28)$$

Here the following reference constants are chosen:

$t^0$  = quarter of the periodic time of the predominant mode of oscillation of the pool filled with water

$L$  = characteristic length of the pool

$w^0$  = maximum wall displacement

$p_1^0$  = maximum over pressure in the blowdown pipe

$\rho^i$  = reference density of water

$c$  = speed of sound in water

$g$  = acceleration of gravity

The following first estimates are used for the other scales. The scale of the rigid wall flow velocity  $V_1^0$  is estimated as the velocity resulting from pressure difference  $p_1^0$  acting over distance  $L$  of the pool water during time  $t^0$ :

$$V_1^0 \approx \frac{p_1^0 t^0}{L \rho^i} \quad (29)$$

Change in water density in the rigid wall flow is estimated from the pressure-density relation (20):

$$\Delta \rho_1 \approx \frac{p_1^0}{c^2} \quad (30)$$

For the flow velocity due to wall flexure it seems obvious to choose

$$V_2^0 \approx \frac{w^0}{t^0} \quad (31)$$

The scale of the pressure resulting from wall flexure is estimated by nondimensionalizing the pressure boundary condition on a moving wall:

$$\rho^i \frac{d^2 w}{dt^2} = -\frac{\partial p_2}{\partial n} \quad \Rightarrow \quad \frac{\rho^i w^0}{t^{02}} \frac{d^2 w^*}{dt^{*2}} = -\frac{p_2^0}{L} \frac{\partial p_2^*}{\partial n^*} \quad (32)$$

From (32) we have

$$p_2^0 \approx \frac{\rho^i w^0 L}{t^{02}} \quad (33)$$

The same result is obtained by thinking of an acceleration magnitude  $w^0 / t^{02}$  acting on a water column of length  $L$ :  $p_2^0 \approx \rho a L = \rho^i w^0 L / t^{02}$ . Note that in estimating  $p_2^0$ , the assumption of incompressible water has been actually used which is, however, a good approximation in the examined case as is shown later.

Change in water density due to wall flexure is also estimated from the pressure-density relation (20):

$$\rho_2^0 \approx \frac{p_2^0}{c^2} = \frac{\rho^i w^0 L}{c^2 t^{02}} \quad (34)$$

Substituting the above estimates of the scales into (27) and (28) we obtain the following dimensionless equations:

$$\begin{aligned} \Pi_1 \frac{\partial \rho_2^*}{\partial t^*} + \nabla^* \cdot \mathbf{V}_2^* + \Pi_2 (\mathbf{V}_2^* \cdot \nabla^* \rho_2^* + \rho_2^* \nabla^* \cdot \mathbf{V}_2^*) + \\ \Pi_3 (\rho_1^* \nabla^* \cdot \mathbf{V}_2^* + \rho_2^* \nabla^* \cdot \mathbf{V}_1^* + \mathbf{V}_1^* \cdot \nabla^* \rho_2^* + \mathbf{V}_2^* \cdot \nabla^* \rho_1^*) = 0 \end{aligned} \quad (35)$$

$$\begin{aligned} \frac{\partial \mathbf{V}_2^*}{\partial t^*} + \Pi_4 (\mathbf{V}_2^* \cdot \nabla^*) \mathbf{V}_2^* + \Pi_5 ((\mathbf{V}_1^* \cdot \nabla^*) \mathbf{V}_2^* + (\mathbf{V}_2^* \cdot \nabla^*) \mathbf{V}_1^*) + \\ \Pi_3 \rho_2^* \left( \frac{\partial \mathbf{V}_1^*}{\partial t^*} + \Pi_5 (\mathbf{V}_1^* \cdot \nabla^*) \mathbf{V}_1^* \right) = -\nabla^* p_2^* + \Pi_6 \nabla^* \cdot \mathbf{T}_2^* + \Pi_7 \rho_2^* \mathbf{g}^* \end{aligned} \quad (36)$$

where

$$\begin{aligned} \Pi_1 = \left( \frac{L}{ct^0} \right)^2, \quad \Pi_2 = \frac{w^0 L}{c^2 t^{02}}, \quad \Pi_3 = \frac{p_1^0}{c^2 \rho^i}, \quad \Pi_4 = \frac{w^0}{L} \\ \Pi_5 = \frac{p_1^0 t^{02}}{L^2 \rho^i}, \quad \Pi_6 = \frac{\mu t^0}{\rho^i L^2}, \quad \Pi_7 = \frac{Lg}{c^2} \end{aligned} \quad (37)$$

Note that in obtaining the dimensionless momentum equation (36), the obvious assumptions  $\Delta \rho_1 \ll \rho^i$  and  $\rho_2^0 \ll \rho^i$  were used already at this stage.

Values of the reference magnitudes for the POOLEX experiments are shown in Table 1 and 2. It can be seen that the changes in density  $\Delta \rho_1$  and  $\rho_2^0$  are negligible compared to the reference density  $\rho^i = 1000 \text{ kg/m}^3$  which was expected due to the low compressibility of water. Values of the dimensionless parameters (37), calculated according to the estimates in Table 1 and 2, are shown in Table 3.

Table 1. Reference constants for the POOLEX experiments.

$L$ [m]	$t^0$ [s]	$c$ [m/s]	$w^0$ [m]	$p_1^0$ [Pa]	$\rho^i$ [kg/m <sup>3</sup> ]	$\mu$ [Ns/m <sup>2</sup> ]	$g$ [m/s <sup>2</sup> ]
1	0.025	1500	0.001	1e5	1000	0.001	9.81

Table 2. Reference magnitudes calculated according to the reference constants in Table 1 for the POOLEX experiments.

$V_1^0$ [m/s]	$\Delta \rho_1$ [kg/m <sup>3</sup> ]	$V_2^0$ [m/s]	$p_2^0$ [Pa]	$\rho_2^0$ [kg/m <sup>3</sup> ]
2.5	4.4e-2	0.04	1600	7.1e-4

Table 3. Values of the dimensionless parameters (37) with the reference magnitudes taken from Table 1 and 2.

$\Pi_1$	$\Pi_2$	$\Pi_3$	$\Pi_4$	$\Pi_5$	$\Pi_6$	$\Pi_7$
7e-4	7e-7	4e-5	1e-3	6e-2	3e-8	4e-6

The values of the dimensionless parameters in Table 3 are small compared to unity which indicates that we can to a good approximation neglect the corresponding terms in (35) and

(36). Let us for now, however, retain the time derivative of  $\rho_2$  in (35), multiplied by  $\Pi_1$ . This leaves us with

$$\frac{\partial \rho_2}{\partial t} + \rho^i \nabla \cdot \mathbf{V}_2 = 0 \quad (38)$$

$$\rho^i \frac{\partial \mathbf{V}_2}{\partial t} = -\nabla p_2 \quad (39)$$

which have been cast back into dimensional form. These are basic equations for compressible, inviscid fluid with convection terms neglected. Eq. (19), (38) and (39) can be combined in order to obtain the wave equation for  $p_2$ :

$$\frac{\partial^2 p_2}{\partial t^2} - c^2 \nabla^2 p_2 = 0 \quad (40)$$

The wave equation (40) is the one used in ABAQUS in the acoustic-structural analysis (see the previous section).

Further simplification is obtained by now dropping also the term multiplied by  $\Pi_1$  from (35). Then we are left with

$$\nabla \cdot \mathbf{V}_2 = 0 \quad (41)$$

$$\rho^i \frac{\partial \mathbf{V}_2}{\partial t} = -\nabla p_2 \quad (42)$$

i.e. an incompressible fluid. By taking the divergence of the momentum equation (42) and using the continuity equation (41), it is seen that  $p_2$  can be described with the simple Laplace equation:

$$\nabla^2 p_2 = 0 \quad (43)$$

Note that although (43) holds for incompressible potential flow, the flow due to wall flexure is not necessary a potential flow (i.e. vorticity is not necessarily zero): (43) results from the fact that the convection terms  $(\mathbf{V}_2 \cdot \nabla) \mathbf{V}_2$  have been dropped from (42).

Results of the above order of magnitude analysis are consistent with those given in Sonin (1980), which can be seen after little manipulation of parameters  $\Pi_1$ ,  $\Pi_2$  and  $\Pi_5$ . The dimensional parameter  $\Pi_1$  is important as it can be used to assess the importance of the compressibility of the fluid. The present analysis shows the well known result that if the propagation time of a pressure disturbance across the system is short compared to the response time of the system, i.e. if  $\Pi_1$  is small, then acoustic effects can probably be neglected (see e.g. Moody, 1990). Note that for the present case the fluid pressure  $p_2$  could be described by the Laplace equation, but we nonetheless solve  $p_2$  in ABAQUS by using the acoustic formulation. That is, we solve the wave propagation phenomena in the wall flexure

problem, but according to the order of magnitude analysis the effect of these phenomena should be small.

The above approximations decouple the solutions of the flow with rigid walls and of the flow due to wall flexure. It should be then allowed to solve the initial flow problem with rigid walls, transfer the transient wall pressure on the coupled fluid-structural model and solve the coupled fluid-structural problem separately from the initial flow problem. After application of the transient wall pressure from flow solution 1, the motion of the walls drives the flow solution 2 through the boundary condition (32). This procedure is the one proposed in Sec. 4.2.

It is worth noting that the parameter  $\Pi_5$  has the highest value in Table 3 and that it's value was estimated perhaps a little nonconservatively. The corresponding term was found to be critical also by Sonin (1980). By using (29), we can rewrite  $\Pi_5$  as

$$\Pi_5 = \frac{V_1^0 t^0}{L} \quad (44)$$

If  $V_1^0$  is now estimated separately as 10 - 20 m/s from the experiments, the value of  $\Pi_5$  becomes nearly unity and the two cross terms  $(\mathbf{V}_1 \cdot \nabla)\mathbf{V}_2$  and  $(\mathbf{V}_2 \cdot \nabla)\mathbf{V}_1$  in the momentum equation might be significant. The cross terms indicate that if the rigid wall flow velocity (or it's gradient) is very large near the walls, be it stationary or transient, even a small velocity wall motion may induce significant pressure variations. In such a case then the present separate solution method would obviously become invalid.

#### 4.2.2.1 Discussion on Boundary Conditions on the Free Surfaces

It is assumed here that the effect of the wall flexure on the pressure applied on the free surfaces of the fluid, i.e. on the gas pressure on the pool surface and inside the blowdown pipe, is negligible. Therefore, pressure boundary condition  $p_2 = 0$  is used on the free surfaces of the wall flexure flow problem (40) or (43). It is also assumed that the effect of the wall flexure on the locations of the free surfaces at different instants of time is negligible.

Therefore, the boundary condition  $p_2 = 0$  should be applied at the current locations of the free surfaces of the rigid wall flow solution. This introduces additional approximation to the calculation with ABAQUS, since there the locations of the free surfaces of the acoustic fluid remain at their initial location during the calculation. Error due to this depends on the size of the bubbles forming in the pool (on the deviation of the free surfaces from their initial location) and is probably not very large for example during the chugging phase, where the steam-water interface oscillates back and forth near the pipe exit. Magnitude of this error could be examined for example by modeling a (stationary) bubble of typical size at the pipe exit in the acoustic domain and by comparing to results without the bubble. Merely extracting the eigenmodes of the coupled acoustic-structural system might suffice.

#### 4.2.2.2 Note on Possible Non-uniformity of the Approximation

Strictly speaking, it seems that we would still need to at least examine whether the problem is regular or singular perturbation problem (Van Dyke, 1975). For example, a classic singular perturbation problem in fluid mechanics results from the high Reynolds number approximation which was actually used here also. There the small parameter (1/Re) multiplies



the viscous terms, having the highest derivatives in the momentum equation. In the approximation the viscous terms are then dropped, but in the full solution the dropped derivatives usually become very large in the boundary layers, making the approximation invalid in these thin regions. In most part of the solution domain, however, the approximation is usually very accurate. It is then natural to ask whether a similar breakdown of the approximation occurs in the present problem and if it does what is its effect on the results.

In the analysis of Sonin (1980), the viscous terms were completely neglected from both solutions 1 and 2, which is a common approximation. Here the viscous terms are linear, which leaves only  $\nabla \cdot \mathbf{T}_2$  in (25). We conclude here only that it seems reasonable to model the wall flexure flow as inviscid, since it is mainly small amplitude oscillatory motion, caused by large portion of the wall moving in phase and most probably governed by inertial forces.

The other dropped terms in (24) and (25) have only first order derivatives. Van Dyke (1975) presents many regular and singular flow problems, though simple ones compared to the case at hand. The loss of the highest derivative is stated as the classical warning for singularity, but other common sources are also mentioned.

#### 4.2.3 Comparison with Two-Way Coupling

The proposed method is first compared with full two-way FSI calculation in a simplified case, for which a schematic is shown in Fig. 7. It is a round water pool with flexible bottom at the centre; cylindrical symmetry is utilized in modeling. The rigid part of the pool is extended in order to damp out high frequency pressure oscillations in the water. At the top centre of the pool, water is blown in from a hole with diameter 200 mm. The flexible bottom is modeled as a steel plate with thickness 25 mm, but with an artificially large density ( $20\,000\text{ kg/m}^3$ ) in order to have a stable two-way coupled calculation. Likewise in order to increase stability, water is modeled as compressible and single-phase. At the inlet, pressure is ramped from zero to a value of 10 kPa during 0.1 s, after which the pressure is held constant. This creates a pressure pulse on the bottom of the pool, caused by bulk flow of water, causing the flexible part to deflect.

Fig. 8 shows the deflection of the centre of the flexible bottom as a function of time for the full two-way coupled calculation as well as for one-way coupled calculations with and without the acoustic fluid medium. It can be seen that the two-way and the one-way coupled calculation with the acoustic fluid agree quite well with each other, whereas the plain one-way coupled calculation differs from these.

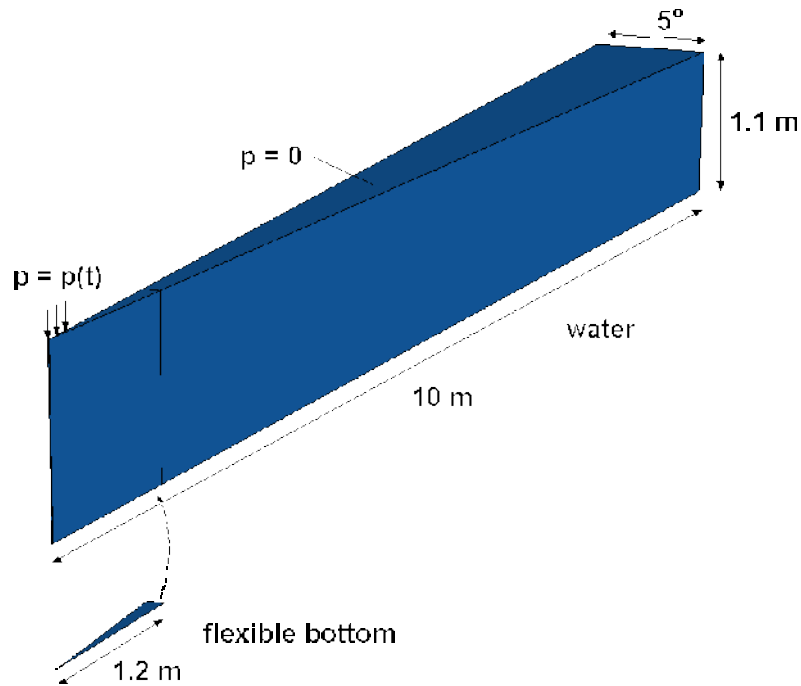


Figure 7. Schematic for a simple test case for comparing the one-way coupled calculation with added mass with full two-way coupled calculation.

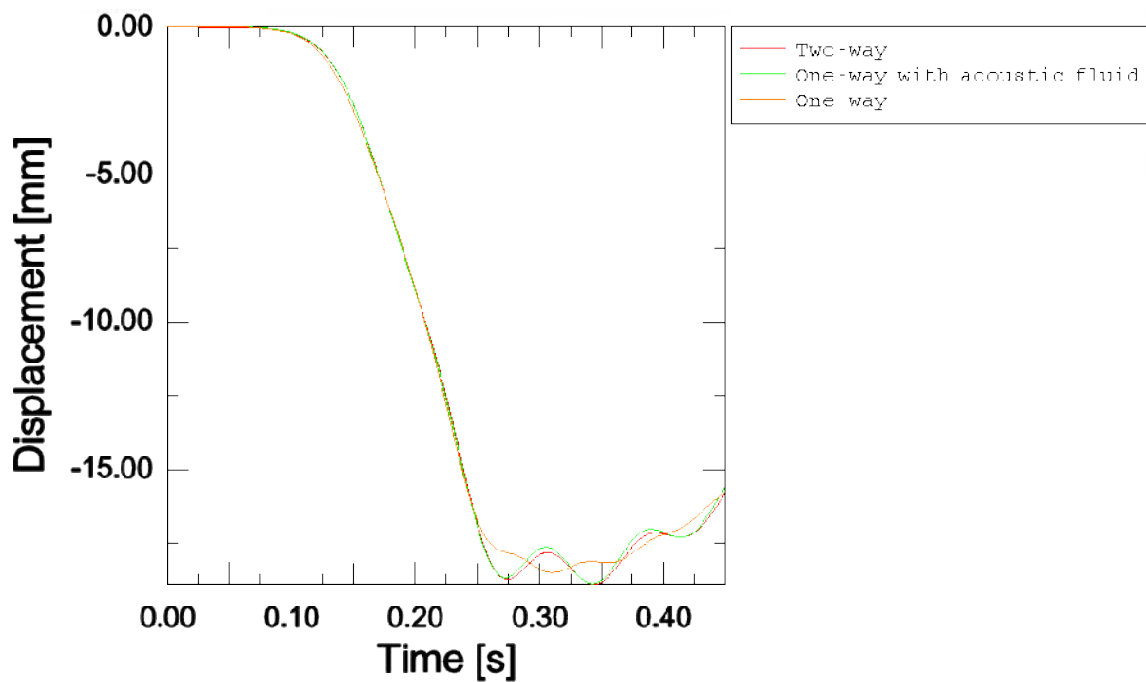


Figure 8. Displacement of the centre of the flexible bottom as a function of time for the two-way and one-way coupled calculations.

#### 4.2.4 Comparison with POOLEX Experiment

For validation of the proposed method, the POOLEX experiment STB-36-5-2, which was performed specifically for validating FSI calculations, is considered. In this experiment, the initial pressure in the blowdown pipe was adjusted so that the pipe is initially completely filled with air, i.e. water level in the pipe is initially right at the outlet of the pipe. The submergence depth of the pipe was 2 meters. As the steam valve is opened, pressure in the pipe is suddenly increased causing rapid growth of air bubble at the pipe outlet. This kind of experiment was chosen, since then condensation effects, which can not be currently modeled accurately, are minimized. For detailed description of the POOLEX facility, see e.g. Laine and Puustinen, (2005).

The CFD and structural models of the facility are those used in the previous work (Timperi et al., 2006), meshes of which are shown in Fig. 9. For the acoustic water, the CFD mesh was imported into ABAQUS as such. The Volume of Fluid (VOF) model of Star-CD was used for tracking the free surface and water and air were modeled as incompressible. With the VOF model in Star-CD, incompressibility is currently required. Pressure measured in the blowdown pipe at its outlet, shown in Fig. 10, was used as a boundary condition. The calculation is approximate also in the sense that the pressure boundary condition already contains the effect of the wall motion. This effect should be, however, small on the gas pressure inside the blowdown pipe.

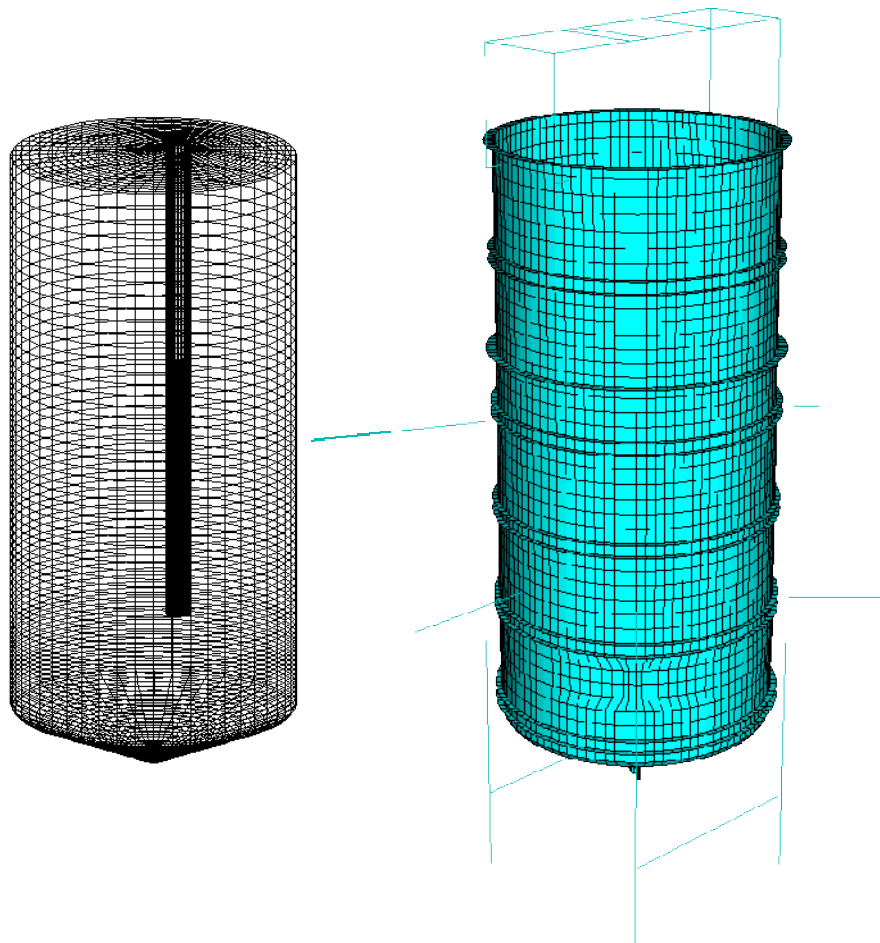


Figure 9. Surface mesh of the CFD model and the structural model of the pool.

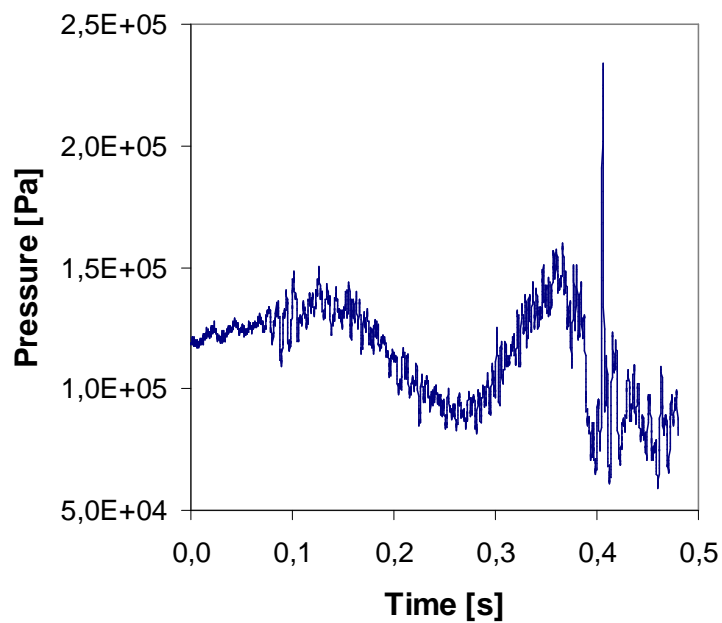


Figure 10. Measured gas pressure inside the blowdown pipe near its exit as a function of time for the POOLEX experiment STB-36-5-2.

Fig. 11 shows the growth of the air bubble at the pipe exit for the simulation and for the experiment. In the experiment the growth of the bubble is somewhat more rapid. In addition, narrow jet starts to penetrate into the water in the experiment at about  $t = 0.2$  s, which is not found in the simulation. The raise of the bubble due to buoyancy at later instants of time seems to be predicted quite well.

Fig. 12 shows pressures on the bottom of the pool below the blowdown pipe for the FSI calculation with added mass and for the experiment. For the calculation, pressures are shown for the CFD model, for the acoustic medium and for the sum of these according to Eq. (21). The pressure of the CFD model shows high-frequency oscillations, which result from the oscillations of the pressure boundary condition (see Fig. 10). The acoustic pressure expectedly oscillates approximately in opposite phase compared to the pressure of the CFD model, so that summing these two quantities produces a smooth curve.

Displacement of the pool bottom centre is shown in Fig. 13 for the one-way coupled calculations with and without the acoustic fluid and for the experiment. Agreement between the calculation with added mass and experiment is reasonably good up to about  $t = 0.35$  s, after which the results deviate. As can be seen from Fig. 11, this is approximately the moment at which water closes the pipe exit and shoots upwards back into the pipe. The results differ after this moment probably because the CFD model ends at the pipe outlet, at which the pressure boundary condition was applied. Therefore, the results should be compared only up to  $t = 0.35$  s. The frequency of motion is, as expected, unrealistically high for the straightforward one-way coupled calculation without added mass.

Note that the displacement in the experiment was estimated from the measured strain at the pool bottom. This could be done according to an experiment in which the static strain and displacement due to the hydrostatic load of water were measured (see Laine and Puustinen, 2005) and according earlier static and dynamic FE simulations.

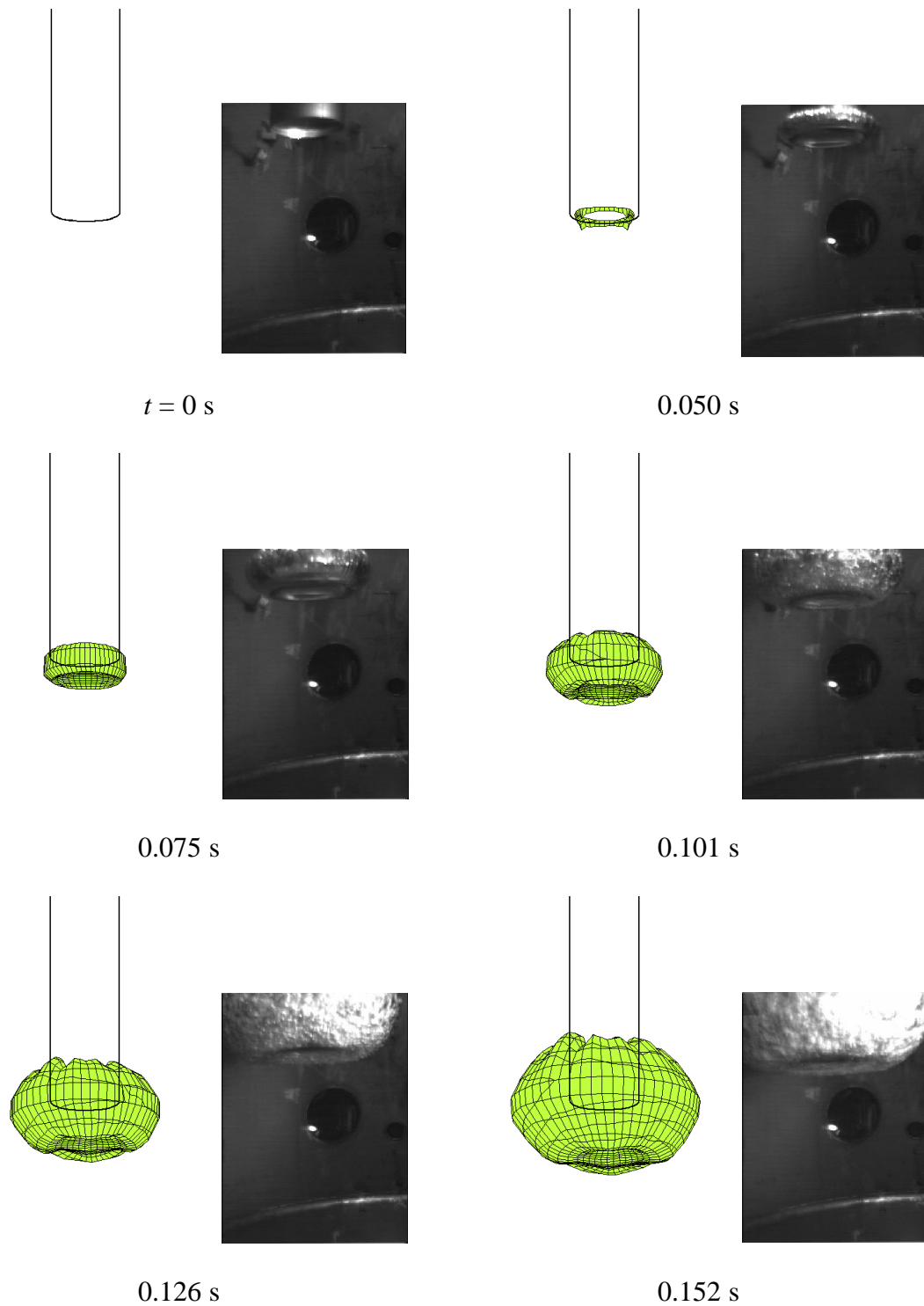


Figure 11. Location of the air-water interface at different instants of time for the simulation and for the experiment STB-36-5-2. Photographs by Nuclear Safety Research Unit, Lappeenranta University of Technology (continues on the following page).

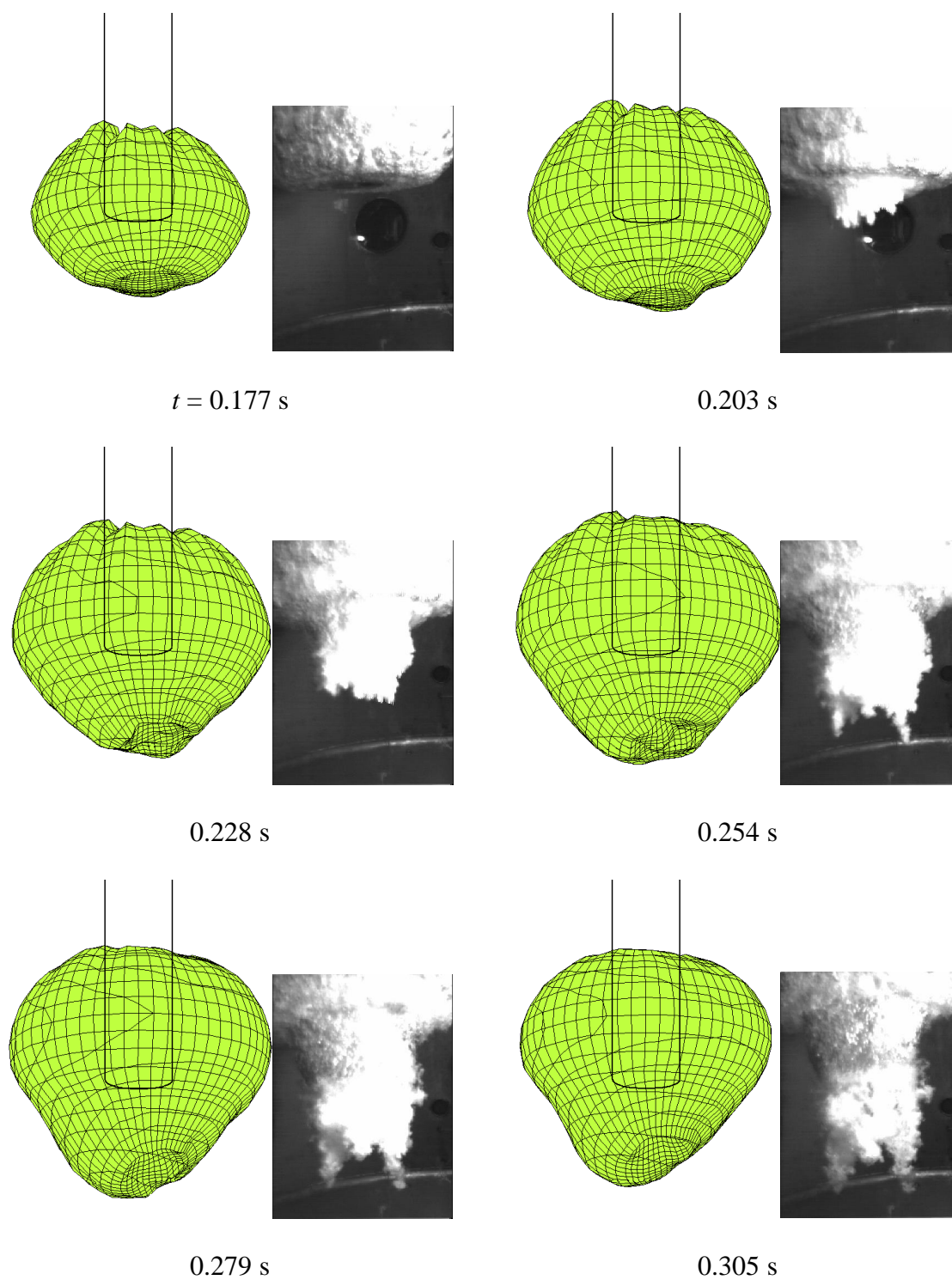


Figure 11. Continues from the previous page.

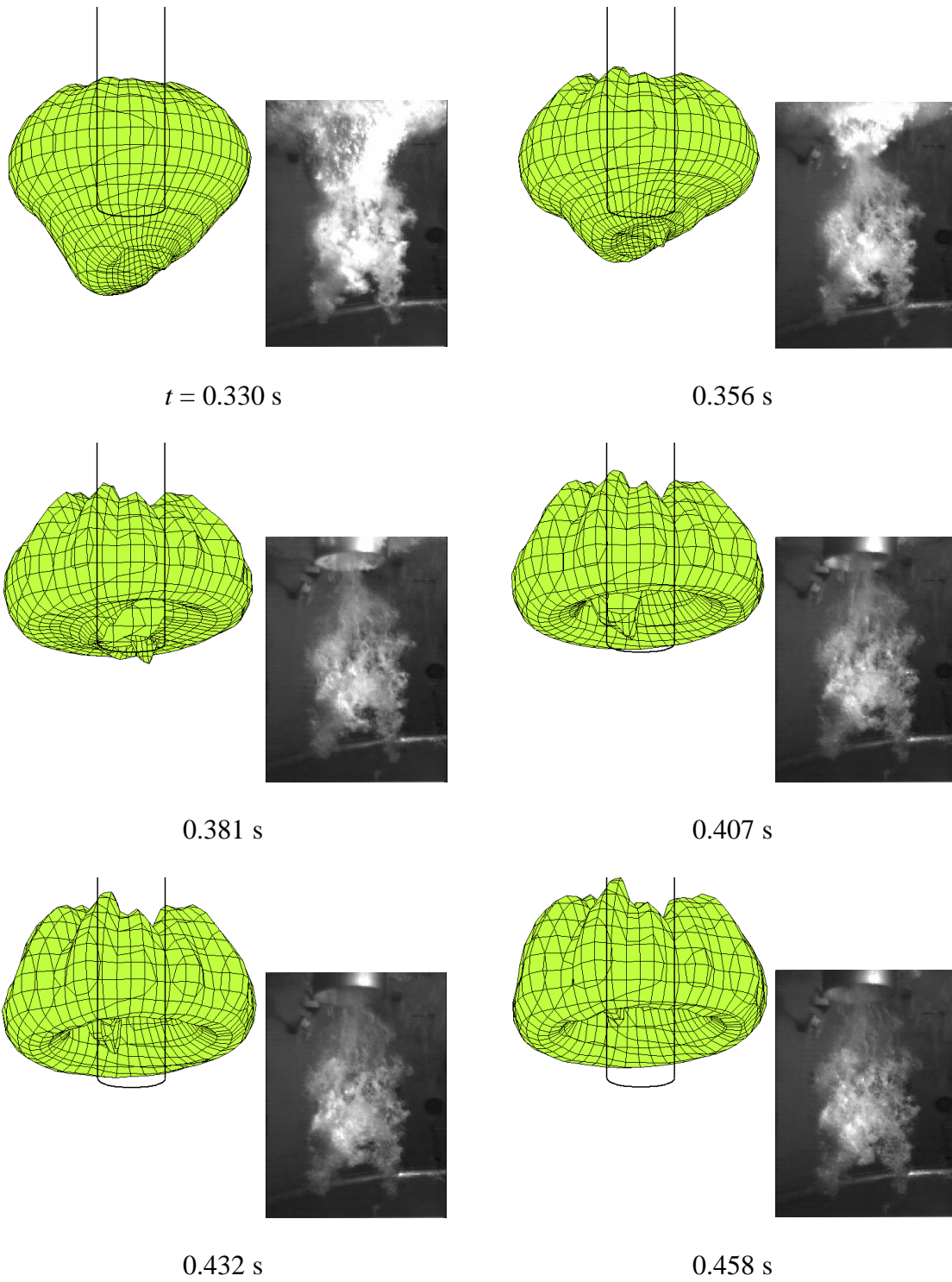


Figure 11. Continues from the previous page.



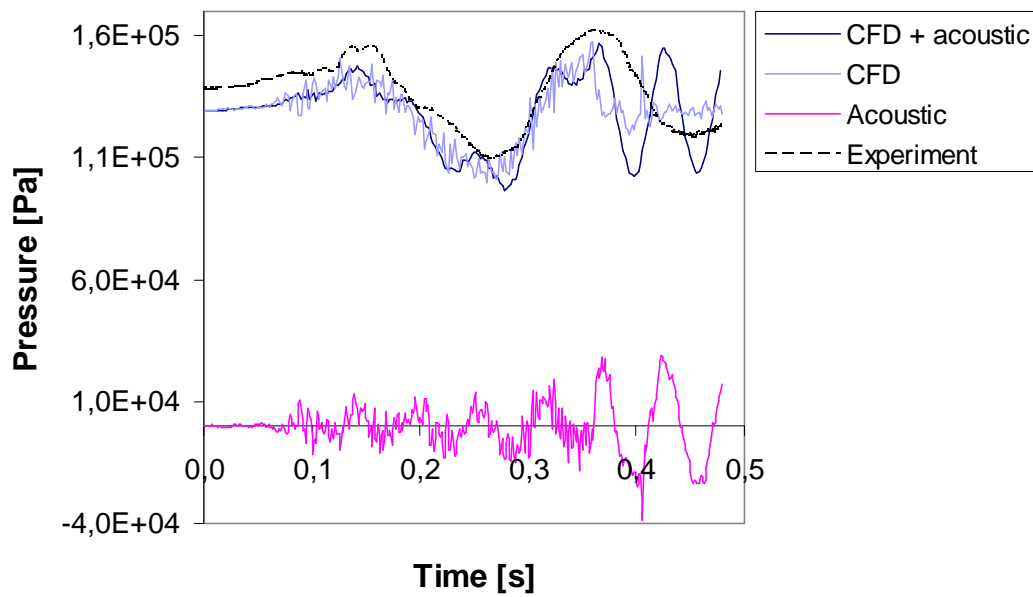


Figure 12. Pressure on the pool bottom below the blowdown pipe as a function of time for the one-way coupled FSI calculation with added mass and for the experiment. The pressures from the CFD and acoustic models show the separate components from the rigid wall flow and from the flow due to wall flexure, respectively.

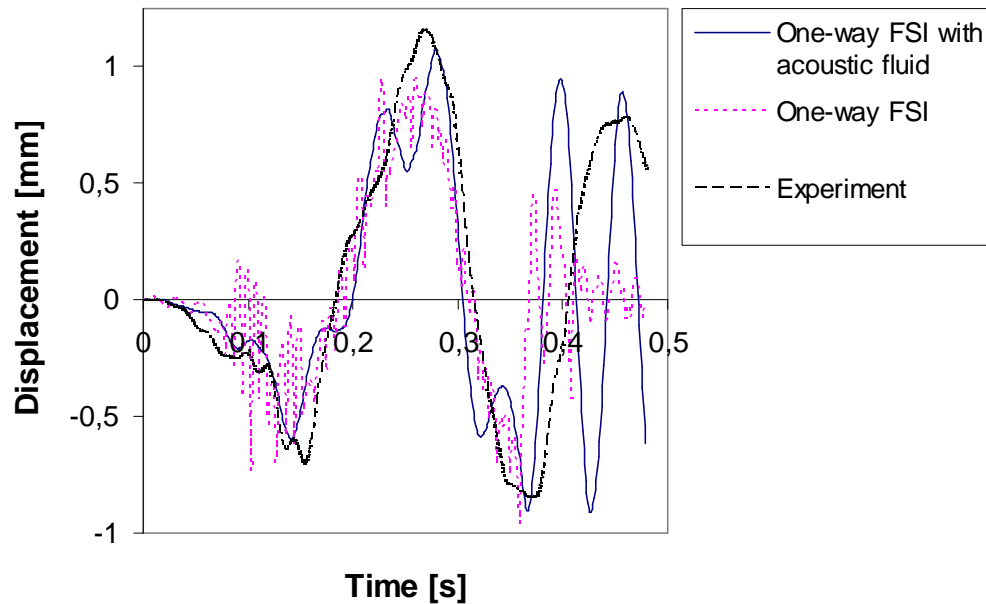


Figure 13. Displacement of the pool bottom centre as a function of time for the one-way coupled FSI calculation with and without added mass and for the experiment.

## 5 Summary and Conclusions

A simplified direct contact condensation model was implemented into the Volume Of Fluid (VOF) model of the Fluent CFD code. Transient three-dimensional test runs for experiments, where steam is blown into a water pool were performed. The implemented model was found to provide too small condensation rate for steam when compared to experiments. In addition, the calculated back and forth oscillation of the steam water interface was much smaller than in the experiments, where rapid condensation of bubbles occurred and water penetrated into the blowdown pipe.

The implemented direct contact condensation model was found to be numerically quite robust. The discrepancies of the model, such as the too small condensation rate, can be to some extent cured by making improvements into the condensation model. In addition, use of finer mesh at the pipe outlet would somewhat improve the numerical results. Use of Euler-Euler multiphase method with full transport equations for both phases would also be advantageous because Euler-Euler model has separate energy equations for both steam and water phases. It seems, however, that only a limited subset of versatile experimental situations can be simulated with reasonable accuracy with such models. Therefore, it is essential to focus on experimental situations that are most important.

As an alternative estimation method of thermohydraulic loads, the SILA code based on potential flow theory, was taken into use. SILA solves the pressure distribution caused by oscillating bubbles in a pool, and is easier to use and more flexible than Method Of Images studied earlier. SILA has been modified for pools without an inner cylinder and test simulations for the POOLEX water pool have been performed.

The MpCCI coupling tool employs a simple explicit coupling scheme, which results in numerical instability in the case of the POOLEX water pool. In order to improve stability, alternatives for implementing an implicit scheme with MpCCI were examined, but it was deemed difficult without access to the source codes. The need for an implicit coupling scheme is widely recognised and vendors of commercial codes will expectedly implement an implicit scheme in their codes in forthcoming years. Also the vendors of MpCCI are currently developing this matter (Wolf, 2006). The commercial ANSYS Multiphysics code seems to already have the implicit capability (ANSYS, 2006).

A method was developed which can be used for analysing two-way FSI problems realistically by using only one-way coupling of CFD and structural analysis codes. In the method the mass of the fluid is accounted for in the structural motion by adding the fluid to the structural model as an acoustic medium and by coupling the acoustic domain with the structure bi-directionally inside ABAQUS. Validity of the method was examined mathematically by an order of magnitude analysis of the fluid equations with promising results. Validation was also performed against a full two-way coupled calculation in a simple test case and against a POOLEX experiment. Both cases showed quite good agreement. Essentially the same method has been validated with good results against a small-scale blowdown experiment earlier by Huber et al. (1979). The method has certain restrictions, the most important one being that the structural displacements have to be sufficiently small. These restrictions do not seem to be too limiting for modeling the POOLEX facility or a real pressure suppression pool. The method may have significance in many other practical applications as well, since only small structural motion is often encountered.

## References

ABAQUS Theory Manual, 2006. Version 6.6. Hibbit, Karlsson & Sorensen Inc. RI.

Abouri, D., Parry, A. and Hamdouni, A., 2004. A stable fluid rigid body interaction algorithm: application to industrial problems. ASME/JSME 2004 Pressure Vessels and Piping Conference **491-1**.

Anon., 2005. Introduction to fluid-structure interaction simulation using ABAQUS and Fluent. 2005 ABAQUS users' conference, Stockholm, Sweden. ABAQUS Inc.

ANSYS web site, 2006. URL: <http://www.ansys.com/solutions/fsi.asp>. ANSYS Inc.

Björndahl, O. and Andersson, M., 1998. Globala vibrationer vid kondensationsförlopp i wetwell orsakade av LOCA i BWR-anläggningar, SKI Rapport 99:3, Sweden, 81 pp.

Calonius, K., Pättikangas, T. and Saarenheimo, A., 2003. Numerical analyses of a water pool under loading caused by large air and steam bubbles, VTT Industrial Systems, Project Report BTUO72-031106, Espoo, Finland, 43 p.

Causin, P., Gerbeau, J.-F. and Nobile, F., 2004. Added-mass effect in the design of partitioned algorithms for fluid-structure problems. ICES report 04-02, The Institute for Computational Engineering and Sciences.

Eerikäinen, L., 1997. Potentiaalteorian mukainen painejakauma nestealtaassa ja sen laskemiseen tarkoitettut SILA-tietokoneohjelmat. Käytönopas. (Pressure distribution in a pool of liquid according to potential theory, and the SILA computer codes for its calculation. User's guide.), VTT Energy, Technical report LVT-1/96, Espoo, Finland, 21 p. (in Finnish)

Giencke, E., 1981. Pressure distribution due to a steam bubble collapse in a BWR pressure suppression pool. Nuclear Engineering and Design 65, 175–196.

Huber, P.W., Kalumuck, K.M. and Sonin, A.A., 1979. Fluid-structure interactions in containment systems: small-scale experiments and their analysis via a perturbation method. 5<sup>th</sup> International Conference on Structural Mechanics in Reactor Technology.

Kim, Y.-S., Park, J.-W. and Song, C.-H., 2004. Investigation of the steam-water direct contact condensation heat transfer coefficients using interfacial transport models, Int. Comm. Heat Mass Transfer, vol. 31, pp 397-408.

Laine, J. and Puustinen, M., 2006. Steam blowdown experiments on chugging. POOLEX 2/2005 research report, Lappeenranta University of Technology, Nuclear Safety Research unit, 40 p. + app. 7 p.

Laine, J. and Puustinen, M., 2005. Condensation pool experiments with steam using DN200 blowdown pipe. POOLEX 4/2004 research report, Lappeenranta University of Technology, Nuclear Safety Research unit, 41 p. + app. 4 p.

Laine, J. and Puustinen, M., 2004. Preliminary condensation pool experiments with steam using DN200 blowdown pipe. POOLEX 1/2004 research report, Lappeenranta University of Technology, Nuclear Safety Research unit.

Laine, J., 2002. Condensation pool experiments with non-condensable gas, Lappeenranta University of Technology, Research Report TOKE-2/2002, 46 p. + app. 14 p.

Matthies, H. and Steindorf, J., 2002. Partitioned but strongly coupled iteration schemes for nonlinear fluid-structure interaction. Institute of Scientific Computing, Technische Universität Braunschweig.

Moody, F.J., 1990. Introduction to unsteady thermofluid mechanics. Wiley.

Pättikangas, T., Timperi, A., Niemi, J. and Narumo, T., 2005. Fluid-structure interaction analysis of a water pool under loading caused by a condensation induced water hammer, VTT Industrial Systems, Research Report BTUO72-051332, Espoo, Finland, 56 p.

The Relap5 Development Team, Relap5/Mod3 Code Manual, Vol. 1: Code Structure, System Models, and Solutions Methods, NUREG/CR-5535, INEL-95/0174, U.S. Nuclear Regulatory Commission, USA, 1985.

Sigrist, J.F. and Abouri, D., 2006. Numerical simulation of a non-linear coupled fluid-structure problem with implicit and explicit coupling procedures. ASME 2006 Pressure Vessels and Piping Conference, PVP2006-ICPVT-11-93107.

Sonin, A.A., 1980. Rationale for a linear perturbation method for the flow field induced by fluid-structure interactions. *Journal of Applied Mechanics* **47** pp. 725-728.

Timperi, A., Pättikangas, T., Niemi, J. and Ilvonen, M., 2006. Fluid-structure interaction analysis of a water pool under loading caused by steam injection, VTT Industrial Systems, Research Report TUO72-056662, Espoo, Finland, 64 p.

Timperi, A., Pättikangas, T. and Hänninen, M., 2005. Joint CFD-FEM Calculations of Pressure Transient in LBLOCA Using APROS, Star-CD and ABAQUS, VTT Industrial Systems, Research Report TUO72-056661, Espoo, Finland, 67 pp.

Timperi, A., Pättikangas, T., Calonius, K., Tuunanen, J., Poikolainen, J. and Saarenheimo, A., 2004. Numerical analyses of a water pool under loadings caused by a condensation induced water hammer, VTT Industrial Systems, Research Report BTUO72-031198, Espoo, Finland, 66 pp.

Van Dyke, M., 1975. Perturbation methods in fluid mechanics. The Parabolic Press, Stanford, California.

Vierendeels, J., Dumont, K., Dick, E. and Verdonck, P., 2005. Analysis and stabilization of fluid-structure interaction algorithm for rigid-body motion. *AIAA Journal* **43**, No. 12.

Wolf, K., Fraunhofer-Institute for Algorithms and Scientific Computing, 2006. Personal communication.

Title	Analysis of Loads and Fluid-Structure Interactions in a Condensation Pool
Author(s)	Antti Timperi, Timo Pättikangas and Jarto Niemi
Affiliation(s)	VTT, Technical Research Centre of Finland
ISBN	978-87-7893-217-4 <i>Electronic report</i>
Date	April 2007
Project	NKS-R / Delipool
No. of pages	41
No. of tables	3
No. of illustrations	13
No. of references	27
Abstract	<p>A simplified direct contact condensation model was implemented into the Volume of Fluid model of the Fluent CFD code. Transient three-dimensional test runs for the POOLEX experiments, where steam is blown into a water pool were performed. The model was found to provide too small condensation rate for steam when compared to experiments. In addition, the calculated back and forth oscillation of the steam water interface was much smaller than in the experiments. The model was found to be numerically quite robust. The discrepancies of the simulation, such as the too small condensation rate, could be to some extent cured by making improvements into the condensation model.</p> <p>As an alternative estimation method of thermohydraulic loads in condensation pools, the SILA code based on potential flow theory, was taken into use. SILA solves the pressure distribution caused by oscillating bubbles in a pool, and is easier to use and more flexible than Method of Images studied earlier. SILA has been modified for pools without an inner cylinder and test simulations for the POOLEX water pool were performed.</p> <p>The MpCCI FSI coupling software employs an explicit coupling scheme, which results in numerical instability in the case of the POOLEX facility. In order to improve stability, ways for implementing an implicit coupling scheme with MpCCI were examined. It was found that such a scheme is difficult to achieve without access to the source codes. An implicit coupling scheme is expected to be available with MpCCI in forthcoming years.</p> <p>A method was developed which can be used for analysing two-way FSI problems realistically by using only one-way coupling of CFD and structural analysis codes. In the method, the mass of the fluid is accounted for in the structural motion by adding the fluid to the structural model as an acoustic medium. Validity of the method was examined with promising results mathematically by an order of magnitude analysis and by comparing numerical results with a full two-way calculation in a simple test case and with a POOLEX experiment. The method has certain restrictions, the most important being that structural displacements have to be sufficiently small. These restrictions do not seem to be too limiting for modeling the POOLEX facility or a real pressure suppression pool. The method may have significance in many other applications as well where structural motion is small but the added mass effect of fluid is significant.</p>
Key words	CFD, FEM, fluid-structure interaction, steam injection, pressure suppression pool